

# Fully adaptive structure-preserving hyper-reduction of parametric Hamiltonian systems

Cecilia Pagliantini\*

Federico Vismara†

August 2023

## Abstract

Model order reduction provides low-complexity high-fidelity surrogate models that allow rapid and accurate solutions of parametric differential equations. The development of reduced order models for parametric *nonlinear* Hamiltonian systems is challenged by several factors: (i) the geometric structure encoding the physical properties of the dynamics; (ii) the slowly decaying Kolmogorov  $n$ -width of conservative dynamics; (iii) the gradient structure of the nonlinear flow velocity; (iv) high variations in the numerical rank of the state as a function of time and parameters. We propose to address these aspects via a structure-preserving adaptive approach that combines symplectic dynamical low-rank approximation with adaptive gradient-preserving hyper-reduction and parameters sampling. Additionally, we propose to vary in time the dimensions of both the reduced basis space and the hyper-reduction space by monitoring the quality of the reduced solution via an error indicator related to the projection error of the Hamiltonian vector field. The resulting adaptive hyper-reduced models preserve the geometric structure of the Hamiltonian flow, do not rely on prior information on the dynamics, and can be solved at a cost that is linear in the dimension of the full order model and linear in the number of test parameters. Numerical experiments demonstrate the improved performances of the fully adaptive models compared to the original and reduced models.

## 1 Introduction

We are interested in the numerical solution of large-scale parametric nonlinear Hamiltonian systems that need to be tested for a large number of parameters. Despite the success of model order reduction for time-dependent problems [3, 18], reduced order models for such systems face little or no computational gain, and the possible onset of numerical instabilities resulting from failing to satisfy the Hamiltonian structure of the flow.

More in details, for any given parameter  $\eta \in \mathbb{R}^\sigma$ ,  $\sigma \geq 1$ , we consider the Hamiltonian system described by the initial value problem: find  $w(\cdot; \eta) : \mathcal{T} := (t^0, \infty) \rightarrow V_{2N} \subset \mathbb{R}^{2N}$  such that

$$\begin{cases} \dot{w}(t; \eta) = J_{2N} \nabla \mathcal{H}_\eta(w(t; \eta)), & t \in \mathcal{T}, \\ w(t^0; \eta) = w^0(\eta) \in V_{2N} \end{cases} \quad (1)$$

where  $\mathcal{H}_\eta : V_{2N} \rightarrow \mathbb{R}$  is the Hamiltonian of the system for any  $\eta$ ,  $V_{2N}$  is a  $2N$ -dimensional vector space, and  $J_{2N}$  is the so-called canonical symplectic tensor

$$J_{2N} := \begin{pmatrix} 0_N & I_N \\ -I_N & 0_N \end{pmatrix} \in \mathbb{R}^{2N \times 2N},$$

with  $I_N, 0_N \in \mathbb{R}^{N \times N}$  denoting the identity and zero matrices, respectively. The operator  $J_{2N}$  identifies a symplectic structure on the phase space of the Hamiltonian system (1). Equivalently, the vector space  $V_{2N}$  can be endowed with a local basis  $\{e_i\}_{i=1}^{2N}$  which is symplectic and orthonormal [4, Chapter 12], that is  $e_i^\top J_{2N} e_j = (J_{2N})_{i,j}$  and  $(e_i, e_j) = \delta_{i,j}$  for all  $i, j = 1, \dots, 2N$ , where  $(\cdot, \cdot)$  is the Euclidean inner product. In this coordinates system the symplectic tensor is related to the so-called symplectic 2-form  $\omega$  by  $\omega(u, v) = u^\top J_{2N} v$  for any  $u, v \in V_{2N}$ . Throughout the paper, we assume also that, for each fixed  $\eta$ , the velocity field of the flow is Lipschitz continuous in the state  $w(\cdot; \eta)$  uniformly with respect to time.

In large-scale simulations, namely when the number  $2N$  of degrees of freedom is large, the computational cost of solving problem (1) for  $p$  instances of the parameter  $\eta$  can be prohibitive. In recent years,

\*Dipartimento di Matematica, Università di Pisa, Italy. Email: [cecilia.pagliantini@unipi.it](mailto:cecilia.pagliantini@unipi.it).

†Centre for Analysis, Scientific computing and Applications, Eindhoven University of Technology, The Netherlands. Email: [f.vismara@tue.nl](mailto:f.vismara@tue.nl).

structure-preserving reduced basis methods [29, 1, 16, 23, 25] have allowed to derive computational models that retain the symplectic structure of the phase space and can be solved efficiently in case of *linear* and *affine* Hamiltonian systems. However, in the presence of *nonlinear* Hamiltonian systems no computational gain is obtained. In a recent work [26] by the authors, a gradient-preserving hyper-reduction algorithm has been developed to efficiently solve nonlinear problems resulting from the symplectic model order reduction of Hamiltonian systems. The idea is to combine a suitable decomposition of the reduced Hamiltonian with empirical interpolation (EIM) [2] to derive an approximate Hamiltonian that can be evaluated at a cost independent of the size of the full order model. The method proposed in [26] can deal, however, with only one parameter at the time. Moreover, it has been observed that the reducibility of the nonlinear operators involved increases as the size of the reduced basis space decreases. Low-dimensional approximation spaces for conservative dynamical systems are achievable only via nonlinear model order reduction. Indeed the slowly decaying Kolmogorov  $n$ -width typical of transport-dominated problems and conservative dynamics [9] makes the use of traditional reduced basis methods based on global approximation spaces ineffective. To address this challenge, symplectic dynamical techniques based on dynamical low-rank approximation have been developed in [23, 25] to evolve the reduced space, but no hyper-reduction has been considered. Additionally, even in the presence of linear Hamiltonian fields, the aforementioned methods achieve a computational complexity of, at least,  $O(Np)$ : for many instances of the parameters, large-scale simulations are thus simply not feasible.

This work proposes to combine symplectic dynamical model order reduction with adaptive gradient-preserving hyper-reduction and parameters sampling to yield efficient reduced order models. The main contributions are:

1. a gradient-preserving hyper-reduction based on empirical interpolation where the EIM space is updated in time via a low-rank correction that minimizes the residual. The adaptive strategy relies on a subsample of parameters chosen as to improve the approximation of the nonlinear term at the current time;
2. a strategy to select parameter subsamples to evolve the reduced basis space and for the adaptive components of the algorithm to improve computational efficiency while ensuring favorable approximability properties;
3. an algorithm to adapt both the dimension of the reduced basis space and of the EIM hyper-reduction space to achieve the desired accuracy in situations where the (numerical) rank of the solution has high variations over time;
4. a novel error indicator to drive the adaptivity based on the error between the Hamiltonian vector field and its local projection onto the tangent space of the reduced basis space, and an algorithm to efficiently evaluate it.

The resulting hyper-reduced models preserve the geometric structure of the Hamiltonian flow, do not rely on prior information on the dynamics, and can be solved at a cost that is linear in the dimension  $N$  of the full order model, linear in the number  $p$  of parameters and that does not depend on the product  $Np$ .

The remainder of the paper is organized as follows. In Section 2 we introduce a matrix-valued formulation of the Hamiltonian dynamical system (1) and discuss its symplectic dynamical low-rank approximation. Section 3 concerns a novel hyper-reduction technique based on empirical interpolation where the EIM basis is adapted over time via a low-rank correction and the adaptation is based on a subsample of the test parameters, whose selection is discussed in Section 3.2. Next, in Section 4 we present an algorithm to adapt the rank of the approximate reduced state and the dimension of the EIM space. An error indicator and another subsamples of the test parameters is used to drive the adaptivity, as discussed in Section 5. The temporal discretization of the resulting hyper-reduced dynamical system is briefly described in Section 6. After summarizing in Section 7 the resulting algorithm and its computational complexity, the proposed methods are tested on a set of numerical experiments in Section 8. Some concluding remarks are presented in Section 9.

## 2 Symplectic dynamical low-rank approximation

We are interested in solving the Hamiltonian system (1) for a given set of  $p$  parameters. The problem can then be recast in a matrix-valued formulation as follows. Let  $\mathcal{W}_k : \mathcal{T} \subset \mathbb{R} \rightarrow V_{2N} \subset \mathbb{R}^{2N}$ ,  $1 \leq k \leq p$ , denote the state variable associated with the  $k$ th parameter  $\eta_k$ , i.e.  $\mathcal{W}_k(t) = w(t; \eta_k)$ , and let  $V_{2N}^p$  be the  $p$ -ary Cartesian power of  $V_{2N}$ . For any  $t \in \mathcal{T}$ , we consider the matrix-valued quantity  $\mathcal{W}(t) = [\mathcal{W}_1(t) \dots \mathcal{W}_p(t)] \in V_{2N}^p \subset \mathbb{R}^{2N \times p}$  and the dynamical system: given  $\mathcal{W}^0 \in V_{2N}^p$  find  $\mathcal{W} \in C^1(\mathcal{T}; V_{2N}^p)$

such that

$$\begin{cases} \dot{W}(t) = X_{\mathcal{H}}(W(t)) := J_{2N} \nabla \mathcal{H}(W(t)), & t \in \mathcal{T}, \\ W(t^0) = W^0, \end{cases} \quad (2)$$

where the Hamiltonian  $\mathcal{H}$  is the vector-valued quantity whose  $k$ th entry is defined as  $(\mathcal{H}(W(t)))_k := \mathcal{H}_{\eta_k}(W_k(t))$ , for any  $k = 1, \dots, p$  and  $t \in \mathcal{T}$ , and its gradient is the matrix

$$\nabla \mathcal{H}(W(t)) = [\nabla_{W_1} \mathcal{H}_{\eta_1}(W_1(t)) | \dots | \nabla_{W_p} \mathcal{H}_{\eta_p}(W_p(t))] \in \mathbb{R}^{2N \times p}.$$

For the model order reduction of (2) we consider a nonlinear approach based on dynamical low-rank approximation [20]. Since we need to preserve the symplectic structure of the phase space, we consider the symplectic approach proposed in [25, 23] where, in addition, we allow the rank of the approximate state to vary in time. Let  $n : \mathcal{T} \rightarrow \mathbb{N}_{>0}$  with  $n(t) \ll N$  for any  $t \in \mathcal{T}$ . We consider a low-rank approximation  $W : \mathcal{T} \rightarrow V_{2N}^p$  of the full order state  $W$  of the form

$$W(t) = A(t)Z(t), \quad \forall t \in \mathcal{T}, \quad (3)$$

where  $Z : \mathcal{T} \rightarrow \mathbb{R}^{2n(t) \times p}$  and  $A : \mathcal{T} \rightarrow \mathbb{R}^{2N \times 2n(t)}$ . The dynamics of the approximate state  $W$  is prescribed in terms of evolution equations for  $A$ , the time-dependent reduced basis, and for  $Z$ , the expansion coefficients in the reduced basis. By imposing that the reduced space spanned by the columns of  $A$  is a symplectic vector space at every time, the approximate reduced dynamics preserves the geometric structure of the full order model. This amounts to approximating  $W$  in the manifold

$$\begin{aligned} \mathcal{M}_n = \{ & W \in \mathbb{R}^{2N \times p} : W = AZ \text{ with } A \in \mathcal{U}_n, \text{ and} \\ & Z \in \mathbb{R}^{2n(t) \times p}, \text{ rank}(ZZ^\top + J_{2n(t)}^\top ZZ^\top J_{2n(t)}) = 2n(t)\}, \end{aligned}$$

where  $\mathcal{U}_n := \{A \in \mathbb{R}^{2N \times 2n(t)} : A^\top A = I_{2n(t)}, A^\top J_{2N} A = J_{2n(t)}\}$ .

## 2.1 Reduced dynamics via Dirac–Frenkel variational principle

To derive the evolution of the approximate state  $W \in \mathcal{M}_n$ , we consider  $T_W \mathcal{M}_n$ , the tangent space of  $\mathcal{M}_n$  at  $W$ , that is the linear subspace of  $V_{2N}^p$  containing the derivatives of all paths on  $\mathcal{M}_n$  passing through  $W$ .

The Dirac–Frenkel variational principle [12, 22] determines the approximate trajectory  $t \mapsto W(t) \in \mathcal{M}_n$  from the condition that the vector field given by the time derivative satisfies, at every time  $t$ ,

$$\dot{W} \in T_W \mathcal{M}_n \quad \text{such that} \quad \dot{W} \in \operatorname{argmin}_{V \in T_W \mathcal{M}_n} \|V - X_{\mathcal{H}}(W)\|,$$

in a suitable norm  $\|\cdot\|$ . In our case, this amounts to projecting the vector field  $X_{\mathcal{H}}$  at  $W$  to the tangent space at  $W$ , namely

$$\dot{W} = \Pi_{T_W \mathcal{M}_n} X_{\mathcal{H}}(W), \quad (4)$$

where  $\Pi_{T_W \mathcal{M}_n} : \mathbb{R}^{2N \times p} \rightarrow T_W \mathcal{M}_n$  is the orthogonal projection with respect to the symplectic 2-form, i.e.,  $\omega(X_{\mathcal{H}} - \Pi_{T_W \mathcal{M}_n} X_{\mathcal{H}}, V) = 0$  for any  $V \in T_W \mathcal{M}_n$ , and it is defined [25, 23] as

$$\Pi_{T_W \mathcal{M}_n}(X_{\mathcal{H}}) = (I_{2N} - AA^\top)(X_{\mathcal{H}}Z^\top + J_{2N}X_{\mathcal{H}}Z^\top J_{2n}^\top)M^{-1}(Z)Z + AA^\top X_{\mathcal{H}}, \quad (5)$$

where  $M(Z) := ZZ^\top + J_{2n}^\top ZZ^\top J_{2n}$ . Using the explicit expression for the projection  $\Pi_{T_W \mathcal{M}_n}$  given in (5) and the factorization (3), the reduced dynamics (4) can be equivalently re-written as

$$\begin{cases} \dot{A} = (I_{2N} - AA^\top)(J_{2N} \nabla \mathcal{H}(AZ)Z^\top + \nabla \mathcal{H}(AZ)Z^\top J_{2n})M^{-1}(Z), & (6a) \\ \dot{Z} = J_{2n} \nabla \mathcal{H}_r(Z), & (6b) \end{cases}$$

where  $\mathcal{H}_r = A^* \circ \mathcal{H}$ . The initial condition is obtained from the projection of  $W(t^0)$  onto  $\mathcal{M}_{n(t^0)}$ . Note that the evolution (6b) of  $Z$  is a Hamiltonian flow with  $2n$  degrees of freedom per parameter, and the Hamiltonian remains an invariant of motion, while  $A(t)$  solution of (6a) belongs to  $\mathcal{U}_{n(t)}$  for any  $t \in \mathcal{T}$ .

It can be shown [25] that, for *linear* systems (1), the computational cost required to solve (6) is linear in the dimension  $N$  of the full order problem and in the number  $p$  of parameters, but it depends on the product  $Np$ . Since both  $N$  and  $p$  can be potentially large, solving the reduced model (6) can still be computationally demanding. Additionally, when the Hamiltonian vector field is a *nonlinear* function of the state, it is well known that the reduced system can be as expensive to solve as the full order one despite dimensionality reduction.

To overcome these limitation we propose: an adaptive gradient-preserving hyper-reduction strategy to efficiently deal with nonlinearities of the Hamiltonian in the evolution (6b) of the coefficients  $Z$ , even in the presence of a large number of parameters (Section 3); a rank-adaptive algorithm to update the dimension of both the reduced basis space and the EIM space to optimize the approximability properties of the reduced state at a low computational cost (Section 4); two parameter sampling strategies to efficiently perform adaptivity of the reduced basis and EIM spaces (Section 3.2 and Section 5).

### 3 Adaptive gradient-preserving empirical interpolation

Let us assume that the Hamiltonian is a nonlinear function of the state, with a general, typically non polynomial, nonlinearity. If the Hamiltonian has also linear or quadratic components, these can be excluded from the hyper-reduction process whenever they can be evaluated at a cost that is independent of  $N$ .

The major computational bottleneck in solving equation (6b) comes from the evaluation of the nonlinear reduced Hamiltonian  $\mathcal{H}_r$ . If traditional hyper-reduction techniques are applied to the full or to the reduced Hamiltonian gradient, the resulting approximate function is no longer a gradient field, leading to unstable or inaccurate approximations [29, 26]. In a recent work [26] by the authors, an adaptive gradient-preserving hyper-reduction technique has been proposed to derive efficient hyper-reduced models that retain the Hamiltonian structure of the flow. However, this method only deals with one parameter at the time. More in details, starting from the reduced order model (6) where the reduced basis  $A \in \mathcal{U}_n$  is assumed to be given and  $Z \in V_{2n}$ , i.e.,  $p = 1$ , [26] proposes a decomposition of the nonlinear (part of the) reduced Hamiltonian of the form

$$\mathcal{H}_r(Z) = \sum_{i=1}^d v_i h_i(AZ) = v^\top h(AZ), \quad \text{for all } Z \in V_{2n}, \quad (7)$$

where  $d \in \mathbb{N}$ ,  $v \in \mathbb{R}^d$  is a constant vector and  $h : \mathbb{R}^{2N \times p} \rightarrow \mathbb{R}^d$ . For hyper-reduction to be effective, the choice of the decomposition should maximize the sparsity of  $h$  as a function of the reduced state  $Z$ , which typically leads to  $d$  scaling with the full order dimension  $N$ . A discussion on this aspect is provided before Section 3.1 and more details can be found in [26, Remark 3.1]. Moreover, examples of Hamiltonians that can be decomposed in such form are given in [21] and [15, Chapter I]. Using the decomposition (7), the gradient of the nonlinear term  $\mathcal{H}_r$  reads  $\nabla \mathcal{H}_r(Z) = A^\top D_h^\top(AZ)v$ , where  $D_h : \mathbb{R}^{2N \times p} \rightarrow \mathbb{R}^{d \times 2N}$  is the Jacobian of  $h$ .

Next step consists in using the empirical interpolation method [2] to approximate the Jacobian mapped to the reduced space, i.e.,  $D_h(A \cdot)A \in \mathbb{R}^{d \times 2n}$ . More in details, let  $m : \mathcal{T} \rightarrow \mathbb{N}_{>0}$  be such that  $m(t) \ll d$  for any  $t \in \mathcal{T}$ . Consider a set of  $m = m(t)$  basis functions arranged as columns of the so-called EIM matrix  $U = U(t) \in \mathbb{R}^{d \times m(t)}$ . Let  $\{i_1, \dots, i_{m(t)}\} \subset \{1, \dots, d\}$  be a set of interpolation indices that form the matrix  $P = P(t) := [\mathbf{e}_{i_1} | \dots | \mathbf{e}_{i_{m(t)}}] \in \mathbb{R}^{d \times m(t)}$  where  $\mathbf{e}_i$  is the  $i$ th unit vector of  $\mathbb{R}^d$ . Assuming  $U$  and  $P$  given, the empirical interpolation operator is defined as

$$\mathcal{I}_m(D_h(AZ)A) = UC, \quad C = C(t) \in \mathbb{R}^{m \times 2n}, \quad (8)$$

with  $C$  obtained from the interpolation constraints  $P^\top D_h(AZ)A = P^\top UC$ . If  $P^\top U$  is non-singular [7, 8], the resulting empirical interpolation of the reduced Jacobian at time  $t \in \mathcal{T}$  reads

$$\mathbb{P}(t)D_h(A(t) \cdot)A(t), \quad \text{where} \quad \mathbb{P} := U(P^\top U)^{-1}P^\top \in \mathbb{R}^{d \times d} \quad (9)$$

is the EIM projection matrix. The EIM projection introduced in (9) can be equivalently seen as an approximation of the nonlinear term  $\mathcal{H}_r$  in (7) by

$$\mathcal{H}_t^{\text{hROM}}(Z) := v^\top \mathbb{P}(t)h(AZ) \quad \text{for all } Z \in V_{2n}, t \in \mathcal{T}, \quad (10)$$

whose gradient is given by  $\nabla \mathcal{H}_t^{\text{hROM}}(Z(t)) = A(t)^\top D_h^\top(A(t)Z(t))\mathbb{P}(t)^\top v$ . This term can typically be evaluated efficiently: if  $d = N$  and the  $i$ th entry of the vector-valued function  $h$  only depends on, for example, the  $i$ th and  $(i + N)$ th components of the state, the Jacobian  $D_h$  is the concatenation of two  $d \times d$  diagonal matrices. This is the case for the Hamiltonian formulation of the Schrödinger equation that will be considered in the numerical experiments of Section 8. In this case, the gradient of the hyper-reduced Hamiltonian can be re-written as  $A^\top D_h^\top(AZ)\mathbb{P}^\top v = \tilde{A}^\top \widetilde{\nabla \mathcal{H}}(AZ)$  where  $\tilde{A} \in \mathbb{R}^{2m \times 2n}$  and  $\widetilde{\nabla \mathcal{H}}(AZ) \in \mathbb{R}^{2m}$  is the gradient of the full order system evaluated only at the rows corresponding to the EIM indices. In general, the complexity of evaluating the hyper-reduced gradient  $\nabla \mathcal{H}_t^{\text{hROM}}$  is independent of the full order dimension  $N$  whenever each component of  $h$  depends on  $s \ll N$  entries of the state, so that the Jacobian matrix  $D_h$  is sparse. This condition is typically ensured by the decomposition (7).

In [26] a strategy to construct the EIM pair  $(U, P)$  is proposed in the case where the reduced basis space is fixed over time and the problem does not depend on parameters, namely when the Hamiltonian system needs to be solved only once. When applied to the parametric case, such strategy requires the construction and update of one EIM pair per parameter. In the presence of a high number of parameters this option is not computationally affordable. In the next section we discuss how to address the parametric hyper-reduction with a gradient-preserving and parameter-efficient adaptive strategy.

### 3.1 Adaptivity of the EIM basis and of the interpolation points

Unlike global reduced basis methods, dynamical low-rank approximation is not data-driven, i.e., it does not rely on an offline phase to build the reduced space. It is then necessary to adapt the EIM space and interpolation indices during the simulation to achieve sufficiently accurate approximations [28, 24].

Let us assume, for the time being, that the EIM pair  $(U, P) \in \mathbb{R}^{d \times m} \times \mathbb{R}^{d \times m}$  is given and that the reduced basis  $A \in \mathcal{U}_n$  is fixed. In this section we propose a strategy to update the EIM pair to the quantity  $(U^{\text{upd}}, P^{\text{upd}}) \in \mathbb{R}^{d \times m_{\text{upd}}} \times \mathbb{R}^{d \times m_{\text{upd}}}$  so that the gradient structure of the Hamiltonian vector field is preserved and the updated EIM space provides a better approximation of the nonlinear Hamiltonian vector field for all test parameters. Let us consider the matrix-valued function  $(A, Z) \in \mathcal{U}_n \times \mathbb{R}^{2n \times p} \mapsto D(A, Z) = D \in \mathbb{R}^{d \times 2np}$ , whose  $k$ th column  $D^{(k)}$  is the reduced Jacobian associated to the  $k$ th parameter, namely

$$D^{(k)} = D_h(AZ_k)A \in \mathbb{R}^{d \times 2n} \quad k = 1, \dots, p, \quad (11)$$

with  $Z_k$  the  $k$ th column of the matrix  $Z \in V_{2n}^p$ . The EIM approximation of  $D$  with the current EIM basis  $U$  and interpolation indices  $P$  is given by  $UC$  as in (8), with coefficient matrix

$$C = (P^\top U)^{-1} P^\top D = [C^{(1)} | \dots | C^{(p)}] \in \mathbb{R}^{m \times 2np}, \quad (12)$$

and  $C^{(k)} := (P^\top U)^{-1} P^\top D^{(k)} \in \mathbb{R}^{m \times 2n}$ . We define the quantity  $R := UC - D \in \mathbb{R}^{d \times 2np}$  as EIM residual.

Two quantities play a crucial role in the proposed EIM update: a parameter subsample and a set of sampling indices. Let us consider a subset of  $p_U^* \leq p$  sampling parameters  $\{\eta_{i_1}, \dots, \eta_{i_{p_U^*}}\} \subset \{\eta_1, \dots, \eta_p\}$  and we define the matrices

$$D^* = [D^{(i_1)} | \dots | D^{(i_{p_U^*})}] \in \mathbb{R}^{d \times 2np_U^*} \quad \text{and} \quad \check{D} = [D^{(i_{p_U^*+1})} | \dots | D^{(i_p)}] \in \mathbb{R}^{d \times 2n(p-p_U^*)}.$$

Analogously one can define  $C^* = (P^\top U)^{-1} P^\top D^* \in \mathbb{R}^{m \times 2np_U^*}$ ,  $\check{C} = (P^\top U)^{-1} P^\top \check{D} \in \mathbb{R}^{m \times 2n(p-p_U^*)}$ , and  $R^* := UC^* - D^* \in \mathbb{R}^{d \times 2np_U^*}$ . We also consider a set of  $m_s \geq m$  sampling indices  $\{i_1, \dots, i_{m_s}\} \subset \{1, \dots, d\}$  and introduce the matrices

$$S = [e_{i_1} | \dots | e_{i_{m_s}}] \in \mathbb{R}^{d \times m_s} \quad \text{and} \quad \check{S} = [e_{i_{m_s+1}} | \dots | e_{i_d}] \in \mathbb{R}^{d \times (d-m_s)}. \quad (13)$$

The updated EIM basis  $U^{\text{upd}}$  is obtained as a rank- $r$  correction of the rows of  $U$  corresponding to the sample indices, that is

$$S^\top U^{\text{upd}} = S^\top U + Q_r, \quad \check{S}^\top U^{\text{upd}} = \check{S}^\top U,$$

where  $Q_r \in \mathbb{R}^{m_s \times m}$  has rank  $r$ . Note that this trivially implies that  $r \leq \min(m_s, m) = m$ . The update  $Q_r$  is chosen to minimize the quantity

$$\sum_{\ell=1}^{p_U^*} \|S^\top (U^{\text{upd}} C^{(i_\ell)} - D^{(i_\ell)})\|_F^2 = \|S^\top (U^{\text{upd}} C^* - D^*)\|_F^2 = \|S^\top R^* + Q_r C^*\|_F^2.$$

In other words, the rank- $r$  update  $Q_r$  minimizes, at the sampling indices  $S$ , the EIM residual associated to the sample parameters  $\{\eta_{i_1}, \dots, \eta_{i_{p_U^*}}\}$ . Clearly, the choice of the sampling indices and parameters is crucial and will be discussed in Section 3.2.

In Proposition 1 we derive the update  $Q_r$  by solving the corresponding minimization problem, for any  $1 \leq r \leq \text{rank}(C^*)$ . First, we recast the problem in an equivalent form as described in the following result.

**Lemma 1.** *Let  $\mathcal{O}(\alpha, \beta) := \|M_1 + \alpha\beta^\top M_2\|_F^2$ , with given  $M_1 \in \mathbb{R}^{q_1 \times g}$  and  $M_2 \in \mathbb{R}^{q_2 \times g}$ . Then, for  $1 \leq r \leq q_2$ , it holds*

$$\min_{(\alpha, \beta) \in \mathbb{V}_r} \mathcal{O}(\alpha, \beta) = \min_{(\alpha, \beta) \in \bar{\mathbb{V}}_r} \mathcal{O}(\alpha, \beta),$$

where

$$\begin{aligned} \mathbb{V}_r &:= \{(\alpha, \beta) \in \mathbb{R}^{q_1 \times r} \times \mathbb{R}^{q_2 \times r}, \text{rank}(\alpha) = \text{rank}(\beta) = r\}, \\ \bar{\mathbb{V}}_r &:= \{(\alpha, \beta) \in \mathbb{R}^{q_1 \times r} \times \mathbb{R}^{q_2 \times r}, \text{rank}(\alpha) = \text{rank}(\beta) = r, \alpha^\top \alpha \text{ diagonal}\}. \end{aligned}$$

*Proof.* Let  $m_1 := \min_{(\alpha, \beta) \in \mathbb{V}_r} \mathcal{O}(\alpha, \beta)$  and  $m_2 := \min_{(\alpha, \beta) \in \bar{\mathbb{V}}_r} \mathcal{O}(\alpha, \beta)$ . Clearly,  $m_1 \leq m_2$  since  $\bar{\mathbb{V}}_r \subset \mathbb{V}_r$ .

Let  $(\bar{\alpha}, \bar{\beta}) \in \bar{\mathbb{V}}_r$  be such that  $\mathcal{O}(\bar{\alpha}, \bar{\beta}) = m_2$ . Let  $\bar{Q}$  be the matrix with orthogonal columns and  $\bar{W}$  the upper triangular with ones on the main diagonal obtained from the QR factorization of  $\bar{\alpha}$  without normalization. Define  $\bar{Z} := \bar{\beta} \bar{W}^\top$ . Then  $(\bar{Q}, \bar{Z}) \in \bar{\mathbb{V}}_r$  and  $\mathcal{O}(\bar{Q}, \bar{Z}) = \mathcal{O}(\bar{\alpha}, \bar{\beta}) = m_2$ , which implies that  $m_2 \leq \mathcal{O}(\bar{Q}, \bar{Z}) = m_1$ . Hence, we can conclude that  $m_1 = m_2$ .  $\square$

**Proposition 1.** Assume we are given  $S \in \mathbb{R}^{d \times m_s}$ ,  $R^* \in \mathbb{R}^{d \times 2np\bar{v}}$ , and  $C^* \in \mathbb{R}^{m \times 2n\tau p\bar{v}}$  with  $r_C := \text{rank}(C^*) \leq m$ . Let  $\mathcal{U}^* \Sigma^* (\mathcal{V}^*)^\top$  be the compact singular value decomposition of  $C^*$ , with  $\mathcal{U}^* \in \mathbb{R}^{m \times r_C}$ ,  $\Sigma^* \in \mathbb{R}^{r_C \times r_C}$ ,  $\mathcal{V}^* \in \mathbb{R}^{2n\tau p\bar{v} \times r_C}$ . Let  $\mathcal{O}(\alpha, \beta) := \|S^\top R^* + \alpha \beta^\top C^*\|_F^2$ . Then, for any  $1 \leq r \leq \text{rank}(S^\top R^* \mathcal{V}^*) \leq r_C$ , the solution of the minimization problem  $\min_{(\alpha, \beta) \in \mathbb{V}_r} \mathcal{O}(\alpha, \beta)$  is

$$\alpha \beta^\top = -(S^\top R^* \mathcal{V}^*)_r (\Sigma^*)^{-1} (\mathcal{U}^*)^\top,$$

where  $(S^\top R^* \mathcal{V}^*)_r$  denotes the  $r$ -truncated SVD of  $S^\top R^* \mathcal{V}^*$ . Moreover, it holds

$$\min_{(\alpha, \beta) \in \mathbb{V}_r} \mathcal{O}(\alpha, \beta) = \|S^\top R^*\|_F^2 - \sum_{i=1}^r \bar{\sigma}_i^2,$$

where  $\bar{\sigma}_1 \geq \dots \geq \bar{\sigma}_r$  are the  $r$  dominant singular values of  $S^\top R^* \mathcal{V}^* \in \mathbb{R}^{m \times r_C}$ . In particular, if  $r = \text{rank}(S^\top R^* \mathcal{V}^*)$ , then  $\alpha \beta^\top = -S^\top R^* (C^*)^\dagger$  and

$$\min_{(\alpha, \beta) \in \mathbb{V}_r} \mathcal{O}(\alpha, \beta) = \|S^\top R^*\|_F^2 - \|S^\top R^* \mathcal{V}^*\|_F^2. \quad (14)$$

*Proof.* Let  $r \in \{1, \dots, m\}$  be fixed and let  $\alpha_i \in \mathbb{R}^{m_s}$  and  $\beta_i \in \mathbb{R}^m$ , for  $i = 1, \dots, r$ , denote the column vectors of  $\alpha$  and  $\beta$ , respectively, so that  $\alpha = [\alpha_1 | \dots | \alpha_r] \in \mathbb{R}^{m_s \times r}$  and  $\beta = [\beta_1 | \dots | \beta_r] \in \mathbb{R}^{m \times r}$ . Owing to Lemma 1, we look for  $(\alpha, \beta)$  in  $\mathbb{V}_r$ . Using the definition of the Frobenius norm and the linearity and cyclic properties of the trace, together with the fact that the columns of  $\alpha$  are orthogonal, the cost function can be rewritten as

$$\begin{aligned} \mathcal{O}(\alpha, \beta) &= \|S^\top R^* + \sum_{i=1}^r \alpha_i \beta_i^\top C^*\|_F^2 \\ &= \|S^\top R^*\|_F^2 + \sum_{i=1}^r \|\alpha_i\|^2 \|(C^*)^\top \beta_i\|^2 + 2 \sum_{i=1}^r \beta_i^\top C^* (S^\top R^*)^\top \alpha_i. \end{aligned} \quad (15)$$

Defining  $\gamma := \Sigma^* (\mathcal{U}^*)^\top \beta \in \mathbb{R}^{r_C \times r}$  we find

$$\mathcal{O}(\alpha, \beta) = \widehat{\mathcal{O}}(\alpha, \gamma) := \|S^\top R^*\|_F^2 + \sum_{i=1}^r \|\alpha_i\|^2 \|\gamma_i\|^2 + 2 \sum_{i=1}^r \gamma_i^\top (S^\top R^* \mathcal{V}^*)^\top \alpha_i.$$

Computing the partial derivatives of  $\widehat{\mathcal{O}}$  with respect to  $\alpha_i$  and  $\gamma_i$ , for  $i = 1, \dots, r$ , and setting them equal to zero we obtain

$$\gamma_i = -\frac{(S^\top R^* \mathcal{V}^*)^\top \alpha_i}{\|\alpha_i\|^2}, \quad S^\top R^* \mathcal{V}^* (S^\top R^* \mathcal{V}^*)^\top \alpha_i = \sigma_i^2 \alpha_i, \quad (16)$$

where  $\sigma_i := \frac{\|(S^\top R^* \mathcal{V}^*)^\top \alpha_i\|}{\|\alpha_i\|}$  and  $\alpha_i \neq 0$  for all  $i$ , otherwise  $\alpha$  would not have rank  $r$ . This shows that  $(\alpha, \beta)$  is a stationary point of  $\mathcal{O}$  if and only if the columns of  $\alpha$  are left singular vectors of  $S^\top R^* \mathcal{V}^*$  and the columns of  $\beta$  are given by  $\beta_i = \mathcal{U}^* (\Sigma^*)^{-1} \gamma_i$ . To determine which choice of  $\alpha_i$  corresponds to the global minimum of  $\mathcal{O}$ , we observe that, by inserting the expression for  $\gamma_i$  from (16) into (15), we get

$$\mathcal{O}(\alpha, \beta) = \|S^\top R^*\|_F^2 - \sum_{i=1}^r \sigma_i^2.$$

Therefore, we select  $\alpha_i$  as left singular vectors of  $S^\top R^* \mathcal{V}^*$  corresponding to the  $r$  largest singular values. Moreover, we may assume that  $r \leq \text{rank}(S^\top R^* \mathcal{V}^*)$ , since including singular vectors corresponding to zero singular values does not affect the cost function. In other words, if  $S^\top R^* \mathcal{V}^* = \overline{\mathcal{U}} \overline{\Sigma} \overline{\mathcal{V}}^\top$  is the singular value decomposition of  $S^\top R^* \mathcal{V}^*$ , we set  $\alpha_i = \overline{u}_i$  for  $1 \leq i \leq r$ , which gives  $\sigma_i = \overline{\sigma}_i$  and

$$\gamma_i = -(S^\top R^* \mathcal{V}^*)^\top \overline{u}_i = -\overline{\mathcal{V}} \overline{\Sigma} \overline{\mathcal{U}}^\top \overline{u}_i = -\overline{\sigma}_i \overline{v}_i.$$

The optimal update  $\alpha \beta^\top$  is then

$$\sum_{i=1}^r \alpha_i \gamma_i^\top (\Sigma^*)^{-1} (\mathcal{U}^*)^\top = -\sum_{i=1}^r \overline{\sigma}_i \overline{u}_i \overline{v}_i^\top (\Sigma^*)^{-1} (\mathcal{U}^*)^\top = -(S^\top R^* \mathcal{V}^*)_r (\Sigma^*)^{-1} (\mathcal{U}^*)^\top.$$

□

In this work, we focus on full-rank updates, namely  $r = r_C$ , which yields  $\alpha\beta^\top = -S^\top R^*(C^*)^\dagger$  and  $S^\top U^{\text{upd}} = S^\top U - S^\top R^*(C^*)^\dagger$ . After  $U$  has been updated to  $U^{\text{upd}}$ , the interpolation indices  $P$  are also modified accordingly: one may either recompute all interpolation indices by applying a greedy algorithm [7] or QDEIM [10]. In this work we use QDEIM, which is based on a QR factorization of  $(U^{\text{upd}})^\top$  with column pivoting, since it enjoys favorable theoretical properties and it is computationally efficient in practice. Another option is to only replace the indices corresponding to the basis vectors that have undergone the largest rotations in the EIM basis update, as suggested in [28, Section 4.1].

### 3.2 Selection of sampling indices and sampling parameters for hyper-reduction

The update of the EIM basis provided in Proposition 1 ensures that, if  $p_U^* = p$ , the updated EIM basis improves the approximation of the nonlinear term at the current time by lowering the residual compared to the original EIM basis. This result is in agreement with the single-parameter case [26, Theorem 4.1]. In particular, using (14) with  $p_U^* = p$ , the residual associated with the updated EIM basis satisfies

$$\begin{aligned} \|U^{\text{upd}}C - D\|_F^2 &= \|S^\top(U^{\text{upd}}C - D)\|_F^2 + \|\check{S}^\top(U^{\text{upd}}C - D)\|_F^2 \\ &= \|S^\top R\|_F^2 - \|S^\top R\mathcal{V}\|_F^2 + \|\check{S}^\top(UC - D)\|_F^2 \\ &= \|S^\top(UC - D)\|_F^2 - \|S^\top R\mathcal{V}\|_F^2 + \|\check{S}^\top(UC - D)\|_F^2 \\ &= \|UC - D\|_F^2 - \|S^\top R\mathcal{V}\|_F^2 < \|UC - D\|_F^2. \end{aligned} \quad (17)$$

If  $p_U^* < p$  instead, the update ensures an improved approximation for the sample parameters but, in general, not for all parameters. Next result gives a constructive way to select  $p_U^*$  sampling parameters such that this requirement is satisfied.

**Proposition 2.** *Assume that  $(U, P)$  is a given EIM pair and that  $S$  is a given matrix of sampling indices. Let  $D$  be a matrix of nonlinear terms, as defined in (11),  $C := (P^\top U)^{-1}P^\top D$  and  $R := UC - D$ . Let us denote with a superscript  $*$  the aforementioned quantities when restricted to a given set of  $p_U^* \leq p$  sampling parameters. If  $U^{\text{upd}}$  is the rank update of the EIM basis  $U$  obtained with  $p_U^*$  parameters and  $r = r_C$ , as described in Proposition 1, then*

$$\|U^{\text{upd}}C - D\|_F < \|UC - D\|_F \iff \delta > 0,$$

where

$$\delta := \|S^\top R\|_F^2 - \|S^\top(R - R^*(C^*)^\dagger C)\|_F^2. \quad (18)$$

*Proof.* The residual associated with the unused  $p - p_U^*$  parameters is

$$\begin{aligned} \|U^{\text{upd}}\check{C} - \check{D}\|_F^2 &= \|S^\top(U^{\text{upd}}\check{C} - \check{D})\|_F^2 + \|\check{S}^\top(U^{\text{upd}}\check{C} - \check{D})\|_F^2 \\ &= \|S^\top U\check{C} - S^\top R^*(C^*)^\dagger \check{C} - S^\top \check{D}\|_F^2 + \|\check{S}^\top \check{R}\|_F^2 \\ &= \|S^\top \check{R}\|_F^2 + \|S^\top R^*(C^*)^\dagger \check{C}\|_F^2 - 2(S^\top \check{R}, S^\top R^*(C^*)^\dagger \check{C})_F + \|\check{S}^\top \check{R}\|_F^2 \\ &= \|U\check{C} - \check{D}\|_F^2 + \|S^\top R^*(C^*)^\dagger \check{C}\|_F^2 - 2(S^\top \check{R}, S^\top R^*(C^*)^\dagger \check{C})_F \\ &= \|U\check{C} - \check{D}\|_F^2 + \|S^\top \check{R} - S^\top R^*(C^*)^\dagger \check{C}\|_F^2 - \|S^\top \check{R}\|_F^2. \end{aligned}$$

Note that  $\|S^\top \check{R}\|_F^2 = \|S^\top R\|_F^2 - \|S^\top R^*\|_F^2$  and

$$\|S^\top R^*(C^*)^\dagger C\|_F^2 = \|S^\top R^* - S^\top R^* \mathcal{V}^*(\mathcal{V}^*)^\top\|_F^2 = \|S^\top R^*\|_F^2 + \|S^\top R^* \mathcal{V}^*\|_F^2,$$

so that  $\|S^\top \check{R} - S^\top R^*(C^*)^\dagger \check{C}\|_F^2 = \|S^\top R - S^\top R^*(C^*)^\dagger C\|_F^2 - \|S^\top R^*\|_F^2 + \|S^\top R^* \mathcal{V}^*\|_F^2$  and

$$\|U^{\text{upd}}\check{C} - \check{D}\|_F^2 = \|U\check{C} - \check{D}\|_F^2 - \delta + \|S^\top R^* \mathcal{V}^*\|_F^2. \quad (19)$$

The conclusion follows by summing identity (17) with  $*$  quantities and (19), which gives  $\|U^{\text{upd}}C - D\|_F^2 = \|UC - D\|_F^2 - \delta$ .  $\square$

The condition  $\delta > 0$  is trivially satisfied when  $p_U^* = p$ , since  $R^* = R$ ,  $C^* = C$  and  $(C)^\dagger C = \mathcal{V}\mathcal{V}^\top$  so that equation (18) yields  $\delta = \|S^\top R\mathcal{V}\|_F^2$ . The result of Proposition 2 suggests a strategy to select both the sampling indices  $S$  and the  $p_U^*$  sample parameters simultaneously. We propose an iterative strategy in which we add one parameter per iteration, as summarized in Algorithm 1. We select  $p_U^*$  parameters via QR factorization of  $Z$  with column pivoting and as sampling indices those associated with the rows of  $R^* \mathcal{V}^*$  of maximum norm. By maximizing  $\|S^\top R^* \mathcal{V}^*\|_F$ , we have that the updated EIM residual associated

to the given set of  $p_U^*$  sample parameters is minimized with respect to the EIM residual obtained with the old EIM basis, as prescribed by (17).

Once the matrix  $S$  of sampling indices has been constructed, we check whether  $\delta$  is positive, namely if  $\|S^\top R\|_F > \|S^\top (R - R^*(C^*)^\dagger C)\|_F$ . If this is the case, the algorithm stops since Proposition 2 ensures that the Frobenius norm of the EIM residual associated to all test parameters has decreased with the update. Otherwise, a new sample parameter is added to the set, and the sampling indices are recomputed. Once the sampling indices  $S$  and the  $p_U^*$  parameters have been selected, the EIM basis is updated with the low-rank correction  $-S^\top R^*(C^*)^\dagger$  as given in Proposition 1. The correction is already available from the computation of  $\delta$  from the previous steps. Note that the evaluation of  $\delta$  requires the knowledge of the EIM basis  $U$  and of the nonlinear matrix  $D$  only at the interpolation and sampling indices, which implies that the selection algorithm is efficient when both  $m$  and  $m_s$  are smaller than  $d$ .

---

**Algorithm 1** Selection of sample indices and parameters and EIM update
 

---

- 1: **procedure** ( $U^{\text{upd}}, P^{\text{upd}}$ ) = EIM\_UPD( $A, Z, U, P, \tau_{m_s}$ )
  - 2:  $p_U^* \leftarrow 0, \delta \leftarrow -1, \tilde{Z} \leftarrow Z$
  - 3: **while**  $\delta < 0$  **do**
  - 4:      $p_U^* \leftarrow p_U^* + 1$
  - 5:     Add one parameter  $\eta_{i_{p_U^*}}$  via pivoted QR of  $\tilde{Z}$  and update  $\tilde{Z}$  with the output of the pivoted QR stopped after one step
  - 6:     Compute  $D^* = [D^{(i_1)} | \dots | D^{(i_{p_U^*})}] \in \mathbb{R}^{d \times 2np_U^*}$  from  $(A, Z)$  as in (11)
  - 7:     Compute  $C^* = (P^\top U)^{-1} P^\top D^* \in \mathbb{R}^{m \times 2np_U^*}$
  - 8:      $[U^*, \Sigma^*, \mathcal{V}^*] = \text{SVD}(C^*)$
  - 9:      $R^* \mathcal{V}^* = U U^* \Sigma^* - D^* \mathcal{V}^*$
  - 10:      $S = v(v > \tau_{m_s})$  with  $v = \text{vecnorm}((R^* \mathcal{V}^*)^\top) \in \mathbb{R}^d$
  - 11:     Compute  $S^\top R^*(C^*)^\dagger = S^\top R^* \mathcal{V}^* \Sigma^{*-1} U^{*\top}$
  - 12:      $\delta \leftarrow \|S^\top R\|_F^2 - \|S^\top R - S^\top R^*(C^*)^\dagger C\|_F^2$
  - 13: **end while**
  - 14:  $S^\top U^{\text{upd}} \leftarrow S^\top U - S^\top R^*(C^*)^\dagger$  and  $\check{S}^\top U^{\text{upd}} \leftarrow \check{S}^\top U$
  - 15: Orthogonalize  $U^{\text{upd}}$
  - 16:  $P^{\text{upd}} \leftarrow \text{QDEIM}(U^{\text{upd}})$
  - 17: **end procedure**
- 

The arithmetic complexity of Algorithm 1 is  $O(Nnp_U^*) + O(dnr_C p_U^*) + O(dm^2) + O(pnp_U^*) + O(pnmm_s)$ , where we recall that  $2N$  is the size of the full order model,  $2n$  is the dimension of the reduced basis space,  $p$  is the number of parameters,  $d$  is the number of terms in the decomposition (7) of the nonlinear Hamiltonian,  $r_C$  is the rank of the matrix  $C$  defined in (12),  $m$  is the size of the EIM basis,  $m_s$  is the number of sampling points (13), and  $p_U^*$  is the number of sampling parameters used to update the EIM basis.

A detailed analysis of the costs is as follows. The pivoted QR of  $Z \in \mathbb{R}^{2n \times p}$  truncated at  $p_U^*$  pivots has complexity  $O(pnp_U^*)$ . Next, to compute the nonlinear snapshot matrix  $D^*$  defined in (11), the reduced Jacobian  $D_h(A \cdot)A$  has to be evaluated at the columns of the matrix  $Z$  associated with  $p_U^*$  sample parameters. Assuming that the number of non-zero entries in each row of  $D_h$  is  $s \ll d$  and that the number of operations needed to compute its entries is constant,  $O(Nnp_U^*)$  operations are required to reconstruct the reduced order solution at the  $p_U^*$  sample parameters and  $O(dnsp_U^*)$  operations are needed for the multiplication of the Jacobi matrix with the reduced basis  $A$ .

In the following, we assume that  $s \leq r_C \leq m$ . Recall that  $m \leq m_s \leq d$ , so that we also have  $s \leq m_s$ . The computation of  $C^*$  requires matrix-matrix multiplications for a computational complexity of  $O(m^3) + O(m^2 n_\tau p_U^*)$ . The SVD of  $C^* \in \mathbb{R}^{m \times 2n_\tau p_U^*}$  is computed with  $O(mnp_U^* \min(m, 2n_\tau p_U^*))$  operations.

The matrix-matrix multiplications involved in the construction of  $R^* \mathcal{V}^*$  have complexity  $O(dmr_C) + O(dnr_C p_U^*)$ , while computing the norm of all  $d$  rows of  $R^* \mathcal{V}^* \in \mathbb{R}^{d \times r_C}$  requires  $O(dr_C)$  operations.

For the evaluation of  $\delta$  defined in (18), one has to compute the EIM residual at the rows corresponding to the sampling indices for all test parameters. Before evaluating  $\delta$  we assemble  $S^\top R^*(C^*)^\dagger C = S^\top R^* \mathcal{V}^* (\Sigma_j^*)^{-1} (U^*)^\top C$ . The matrix  $S^\top R^* \mathcal{V}^*$  is already available from line 9, and the matrix-matrix product with  $(\Sigma_j^*)^{-1} (U^*)^\top$  has complexity  $O(m_s r_C m)$ . After that we evaluate  $S^\top R = S^\top U C - S^\top D = S^\top U (P^\top U)^{-1} (P^\top D) - S^\top D$ : the matrices  $D^*$  and  $C^*$  are already available from lines 8 and 9. Therefore,  $S^\top R^*$  can be computed with complexity  $O(mm_s n p_U^*)$  by multiplying  $S^\top U$  by  $C^*$  and then subtracting  $S^\top D^*$ . In order to compute  $S^\top \check{R}$ , one has to build  $P^\top \check{D}$  and  $S^\top \check{D}$  first. Repeating the argument of lines 8 and 9 with  $m$  or  $m_s$  in place of  $N$  and  $d$ , and with  $p - p_U^*$  in place of  $p_U^*$ , the computational



complexity for computing  $P^\top \check{D}$  is  $O((p - p_U^*)mn) + O((p - p_U^*)snm)$ , while computing  $S^\top \check{D}$  requires  $O((p - p_U^*)m_s n) + O((p - p_U^*)snm_s)$  operations. The number of operations required by the matrix-matrix products involved in the computation of  $S^\top \check{R}$  is  $O(m_s m^2) + O(m_s mn(p - p_U^*))$ . Therefore,  $S^\top R$  can be computed in  $O(m_s m^2) + O(m_s mnp)$  operations.

Then, at line 12, the multiplication by the matrix  $C$ , which is available from line 10, has complexity  $O(m_s mnp)$  and the two Frobenius norms are computed in  $O(m_s np)$  operations.

Finally the update is performed at line 14 (complexity  $O(m_s m)$ ), the columns of the resulting matrix are re-orthogonalized ( $O(dm^2)$ ) and the EIM interpolation indices are recomputed (also  $O(dm^2)$  with QDEIM).

## 4 Adaptivity of the approximation rank and of the EIM space dimension

There are two quantities that play a crucial role in the accuracy of the approximation introduced by the model order reduction and hyper-reduction and in the efficiency of the corresponding algorithms: the dimension of the reduced basis space and the dimension of the EIM space. It is indeed desirable that both these dimensions are significantly smaller than the dimension of the full order model to ensure a computational gain. On the other hand, the choice of the reduced space dimension should be strictly related to the numerical rank of the full solution: a too small reduced space might yield an inaccurate representation of the full order dynamics, while a too large value might lead to over-approximation and little or no runtime gain. Moreover, the numerical rank of the full order solution is likely to change over time depending on the variability of the solution as a function of the parameter and on the nonlinearity of the dynamics.

We propose an algorithm to update the dimension of both the reduced space and of the EIM space at the beginning of each temporal sub-interval introduced by the temporal discretization of the dynamics. Let us consider the splitting of the time domain  $\mathcal{T}$  into the union of intervals  $\mathcal{T}_\tau := (t^\tau, t^{\tau+1}]$ ,  $\tau = 0, \dots, N_t - 1$ , with  $t^{N_t} := T$ , and let the local time step be defined as  $\Delta t_\tau = t^{\tau+1} - t^\tau$  for every  $\tau$ . We assume that the dimensions of the reduced and EIM space can change only at the discrete time instants  $\{t^\tau\}_{\tau=1}^{N_t-1}$ . In each temporal subinterval  $\mathcal{T}_\tau$ , the dimension of the reduced space is denoted by  $2n_\tau$  while the dimension of the EIM space is  $m_\tau$ , the approximate reduced state at time  $t^\tau$  is  $W_\tau$  and its low-rank factors are  $A_\tau$  and  $Z_\tau$ .

### 4.1 Rank adaptivity

At the initial time, the rank  $n_0$  of the approximate state  $W^0$  is determined in such a way that  $W^0$  approximates the exact initial condition with a chosen accuracy. As time evolves, an error indicator is used to check the quality of the current approximation and, based on a certain criterion, the reduced basis space is enlarged or reduced. The choice of a suitable error indicator is a crucial feature of the rank adaptivity algorithm: it should provide an accurate indication of the current approximation error with respect to the full order solution and, at the same time, it should be computed at a relatively low computational cost.

Rank-adaptation has received considerable attention in recent years. A family of works proposes adaptive techniques based on the spectral properties of the approximate solution: a recompression of the approximate tensor decomposition of the solution is proposed in [11] for the numerical solution of the Vlasov-Poisson equation; in [5] the rank of the approximation is doubled at each time step based on past information of the solution and then truncated SVD is applied; in [19] an additional singular value is propagated in time and used as an indicator to select the rank of the solution at the new time step. The aforementioned methods are relatively cheap in terms of computational time but do not provide any indication on the error with respect to the full order solution. Moreover, they do not consider parameter-dependent problems and cannot ensure that the geometric structure of the problems at hand is preserved. A rank-adaptive, structure-preserving reduced basis method was introduced in [17], with an error indicator based on the linearized residual of the full order model. Although this quantity provides an accurate estimate of the error between the reduced and the full order solution, its computation requires to solve a linear system of dimension  $2N$  for all test parameters. In many practical situations this is simply not affordable. Another family of works [6, 13] proposes to consider the angle between the velocity of the flow, the Hamiltonian vector field  $X_{\mathcal{H}} = J_{2N} \nabla \mathcal{H}$  in our case, and its projection onto the tangent space to  $\mathcal{M}_n$ . The rationale behind this choice is that, if the reduced space is able to accurately capture the full dynamics, then the full order Hamiltonian vector field is ‘‘almost parallel’’ to its projection. With

our notation, the angle at  $W \in \mathcal{M}_n$  is defined as

$$\theta(W) = \arccos\left(\frac{\|\Pi_{T_W \mathcal{M}_n} X_{\mathcal{H}}(W)\|_F}{\|X_{\mathcal{H}}(W)\|_F}\right), \quad (20)$$

and we let  $\theta_\tau := \theta(W_\tau)$  denote the value obtained by replacing in (20) the approximate state  $W$  with its time discretization at time  $t^\tau$ , that is  $W_\tau$ . This quantity can be evaluated at a relatively low computational cost since  $\Pi_{T_{W_\tau} \mathcal{M}_n} X_{\mathcal{H}}(W_\tau) = Y_A(A_\tau, Z_\tau)Z_\tau + A_\tau A_\tau^\top X_{\mathcal{H}}(W_\tau)$  where  $W_\tau = A_\tau Z_\tau$  and  $Y_A(A, Z)$  denotes the right-hand side of (6a); thereby

$$\|\Pi_{T_{W_\tau} \mathcal{M}_n} X_{\mathcal{H}}(W_\tau)\|_F^2 = \|Y_A(A_\tau, Z_\tau)Z_\tau\|_F^2 + \|A_\tau^\top X_{\mathcal{H}}(W_\tau)\|_F^2.$$

Since the quantities involved are already available from the solution of the reduced dynamics (6), the angle (20) can be computed in  $O(Npn_\tau)$  operations. Although this might still be expensive when both  $p$  and  $N$  are large, one may evaluate the angle based on a subset of  $p_A^*$  parameters rather than on all  $p$  parameters, with a computational complexity of  $O(Np_A^*n_\tau)$ . We will discuss this option in Section 5. Moreover, the angle (20) provides an indicator related to the error between the approximate and full order solution, see Proposition 3. However, such error indicator shows some limitations at least in some numerical tests (see Section 8). Indeed, using an angle to determine when the approximation space needs to be changed does not appear to be a robust measure of the approximation error, hence making difficult to set a criterion/tolerance to determine when the approximation has deteriorated. This is further exacerbated by the fact that this approach does not take into account the time evolution of the approximate solution, but only its value at a given time instant.

To overcome the limitations of the currently available rank-adaptive algorithms, we propose an error indicator which is still related to the projection error of the Hamiltonian vector field, but defined as

$$r_\tau := \sum_{\ell=\bar{\tau}}^{\tau} (t^{\ell+1} - t^\ell) \tilde{r}_\ell, \quad (21)$$

where  $\tilde{r}_\ell := \tilde{r}(W_\ell)$ ,  $t^{\bar{\tau}}$  is the time when the last update was performed, and

$$\tilde{r}(W) := \|X_{\mathcal{H}}(W) - \Pi_{T_W \mathcal{M}_n} X_{\mathcal{H}}(W)\|_F, \quad \forall W \in \mathcal{M}_n. \quad (22)$$

The quantity (21) approximates the time integral of the projection error of the Hamiltonian vector field between  $t^{\bar{\tau}}$  and  $t^\tau$ , thus, unlike  $\theta_\tau$ , taking into account the evolution of the approximation error. The complexity of computing  $\tilde{r}_\ell$  at a given time step is again  $O(Npn_\tau)$ , so that the same considerations made for  $\theta_\tau$  also apply here. Moreover, although (21) does not provide a direct indication of the approximation error introduced by dimensionality reduction, the following result holds.

**Proposition 3.** *Let  $\bar{t} \geq t_0$  be fixed and let  $E(t)$  denote the error between the (hyper-)reduced and full order solutions, i.e.,  $E(t) := \mathcal{W}(t) - W(t)$  for any  $t > \bar{t}$ . Let the error indicators  $\theta$  and  $\tilde{r}$  be defined as in (20) and (22), respectively. Then*

$$\begin{aligned} \|E(t)\|_F &\leq \|E(\bar{t})\|_F e^{L(t-\bar{t})} + \int_{\bar{t}}^t \tilde{r}(W(\tau)) e^{L(t-\tau)} d\tau \\ &= \|E(\bar{t})\|_F e^{L(t-\bar{t})} + \int_{\bar{t}}^t \|\nabla \mathcal{H}(W(\tau))\|_F \sin(\theta(W(\tau))) e^{L(t-\tau)} d\tau, \end{aligned}$$

where  $L = \left(\sum_{k=1}^p \ell_k^2\right)^{1/2}$  and  $\ell_k$  is the Lipschitz continuity constant of the Hamiltonian vector field  $X_{\mathcal{H}_{n_k}}$  associated with the  $k$ th parameter.

*Proof.* The evolution of the error can be written as

$$\dot{E} = \dot{\mathcal{W}} - \dot{W} = X_{\mathcal{H}}(\mathcal{W}(t)) - X_{\mathcal{H}}(W(t)) + X_{\mathcal{H}}(W(t)) - \Pi_{T_W \mathcal{M}_n} X_{\mathcal{H}}(W(t)).$$

Since  $d_t \|E(t)\|_F \leq \|\dot{E}(t)\|_F$ , it holds  $d_t \|E(t)\|_F \leq L \|E(t)\|_F + \tilde{r}(W(t))$  and the result follows from Grönwall's lemma [14]. Moreover, it can be easily shown that  $\tilde{r}(W) = \|\nabla \mathcal{H}(W)\|_F \sin(\theta(W))$ , because  $\Pi_{T_W \mathcal{M}_n}$  is an orthogonal projection with respect to the Frobenius norm.  $\square$

This result shows that both  $\theta_\tau$  and  $r_\tau$  provide approximations to an upper bound of the error. Therefore, we suggest the following procedure for rank adaption. Assume that the last rank update has been performed at time  $t^{\bar{\tau}}$  and  $\bar{e} := e_{\bar{\tau}}$  is the value of the error indicator at the last update, where  $e$  denotes either  $\theta$  or  $r$ . As suggested in [17], the rank update is performed when

$$e_\tau \geq \bar{e} K(\lambda), \quad \text{where} \quad K(\lambda) := C_1 C_2^\lambda, \quad C_1, C_2 \in \mathbb{R}_+, \lambda \in \mathbb{N}. \quad (23)$$

In case this criterion is satisfied, the rank of the reduced solution is increased: the reduced basis is augmented with the space directions in which the projection error  $E_P(W_\tau) := X_{\mathcal{H}}(W_\tau) - \Pi_{T_W \mathcal{M}_n} X_{\mathcal{H}}(W_\tau)$  is currently worst approximated. More in details, we compute the singular value decomposition of  $E_P(W_\tau)$  and add to the reduced basis the  $n_{\tau+1} - n_\tau$  dominant singular vectors together with their symplectic duals. The new vector of coefficients is defined as the projection of the old coefficients onto the new reduced basis:  $Z_\tau^{\text{new}} = (A_\tau^{\text{new}})^\top A_\tau Z_\tau$ . The number of new basis vectors to be added to the old reduced basis can either be fixed (e.g., by adding one pair  $(v, J_{2N}^\top v)$  of basis vectors at each adaption) or determined based on a suitable tolerance.

It is important to note that the matrix  $S$  is ill-conditioned after the rank update, so that numerical inaccuracies may arise when solving the evolution equation for the reduced basis. For this reason, a suitable regularization needs to be performed before inverting  $S$ , as explained in [17, Section 4]. We point out that decreasing the size of the reduced basis space is a simpler task since one can look at the spectrum of the reduced state and remove the modes associated with the singular values smaller than a certain value.

## 4.2 Adaptation of the dimension of the EIM space

Finally, we discuss on the selection of the dimension of the EIM space. To initialize the EIM pair  $(U_0, P_0)$ , we collect instances of the reduced Jacobian at the initial time in the matrix  $D_0 := D_h(A_0 Z_0) A_0 \in \mathbb{R}^{d \times 2n_0 p}$ , assuming that  $D_0 \neq 0$ . If this is not the case, the reduced system (6) is solved without hyper-reduction for  $\Delta_0$  time steps, and  $t^{\Delta_0}$  is then taken as initial time for the adaptive EIM strategy. The initial EIM basis  $U_0 \in \mathbb{R}^{d \times m_0}$  is computed via truncated SVD of  $D_0$  to achieve a certain accuracy, while the matrix of interpolation points  $P_0$  is obtained from  $U_0$  via, for example, QDEIM. At the subsequent time steps, the EIM basis is adapted with a low-rank correction as described in Section 3.1. Here we assume that the EIM update is performed at each time step. However, the proposed strategy can easily be extended to a framework where the EIM basis and indices are updated every  $\Delta > 1$  time steps. Although the EIM basis is in principle adapted at each time, we propose to update its dimension only when the rank of the reduced solution is updated, namely based on criterion (23). The rationale is that hyper-reduction is performed on the nonlinear Jacobian mapped to the reduced space: as the reduced space gets larger, it has been observed that the rank of the nonlinear operator increases as well [26, Figure 4].

More in details, whenever the rank of the approximate state  $W$  changes, the EIM basis is re-computed via truncated SVD, based on a given tolerance  $\tau_m$ , of the snapshot matrix of the reduced Jacobian evaluated at the reduced solution  $A^{\text{new}} Z^{\text{new}}$ , where  $A^{\text{new}}$  and  $Z^{\text{new}}$  are the reduced basis and coefficient matrix after the rank update, respectively. In principle one can use subsampling techniques and perform the update based on the matrix  $Z^*$  collecting a subset of the columns of  $Z$ ; the construction of  $Z^*$  will be discussed in Section 5. The rank-adaptive procedure is summarized in Algorithm 2.

---

**Algorithm 2** Rank update at fixed time  $t = t^\tau$

---

- 1: **procedure**  $(A^{\text{new}}, Z^{\text{new}}, U, P) = \text{RANK\_UPDATE}(A, Z, Z^*, \tau_m)$
  - 2:   Form  $A^{\text{new}}$  by increasing  $A$  with the first  $n_{\tau+1} - n_\tau$  singular vectors of  $E_P(W^*)$  where  $W^* = AZ^*$
  - 3:    $Z^{\text{new}} \leftarrow (A^{\text{new}})^\top AZ$
  - 4:   Compute  $U$  via truncated SVD of  $D(A^{\text{new}}, (Z^{\text{new}})^*)$  (11) with tolerance  $\tau_m$
  - 5:    $P \leftarrow \text{QDEIM}(U)$
  - 6: **end procedure**
- 

## 5 Parameters sampling for adaptivity

Even if the size of the reduced basis space  $n(t)$  satisfies  $n(t) \ll N$ , for all  $t \in \mathcal{T}$ , the evolution of the reduced basis and the evaluation of the error indicator for the rank update require evaluating the full order Hamiltonian vector field  $X_{\mathcal{H}}$  at the reduced solution for all test parameters. The computational complexity of these operations scales with the product  $Np$ . In order to mitigate the computational burden of these operations, we propose to select a subset of  $p_A^* < p$  sample parameters  $\tilde{\eta}^* = \{\eta_{i_1}, \dots, \eta_{i_{p_A^*}}\}$ . In particular, for a given choice of the sample parameters at time  $t^\tau$ , we consider the submatrix  $Z_\tau^*$  containing the columns of the approximate coefficients  $Z_\tau$  of indices  $\{i_1, \dots, i_{p_A^*}\}$  in the rank update Algorithm 2, and in the evolution of the reduced basis (6a). In this way, all the operations with complexity  $O(Np)$  have arithmetic complexity  $O(Np_A^*)$ .

To select the sample parameters, we propose to compute the QR factorization of  $Z_\tau$  with column pivoting. The idea is that the reduced space is evolved by only considering the parameters that are

“most relevant” to the dynamics. Typically, we would like to have  $p_A^*$  much smaller than the number of test parameters  $p$ , but we require that  $p_A^* \geq n_\tau$ , which is a necessary condition for  $Z_\tau^*$  to satisfy the rank condition  $\text{rank}(Z_\tau^* Z_\tau^{*\top} + J_{2n_\tau}^\top Z_\tau^* Z_\tau^{*\top} J_{2n_\tau}) = 2n_\tau$ .

With the proposed algorithm, the hyper-reduced model in the temporal interval  $\mathcal{T}_\tau$  reads

$$\begin{cases} \dot{A} = (I_{2N} - AA^\top)(J_{2N}\nabla\mathcal{H}(AZ^*)(Z^*)^\top + \nabla\mathcal{H}(AZ^*)(Z^*)^\top J_{2n_\tau})M^{-1}(Z^*), & (24a) \\ \dot{Z} = J_{2n_\tau}\nabla\mathcal{H}_\tau^{\text{hROM}}(Z), & (24b) \end{cases}$$

where  $\mathcal{H}_\tau^{\text{hROM}}$  is the hyper-reduced Hamiltonian derived as in Section 3 with the subscript  $\tau$  referring to the EIM approximation in the current temporal sub-interval  $\mathcal{T}_\tau$ , and  $2n_\tau$  is the dimension of the current reduced basis space obtained with the rank-adaptive algorithm. Note that the approximate reduced model (24) retains the geometric structure of the full order model.

## 6 Temporal discretization of the hyper-reduced model

For the numerical time integration of the hyper-reduced model (24), we adopt the temporal integrator proposed in [25]. The idea is to combine a symplectic temporal integrator for the evolution (24b) of the expansion coefficient with a time discretization of the basis evolution (24a) able to preserve the ortho-symplectic constraint.

In each temporal sub-interval  $\mathcal{T}_\tau = (t^\tau, t^{\tau+1}]$ , given the approximate reduced basis  $A_\tau$ , the method constructs a local retraction  $\mathcal{R}_{A_\tau}$  so that  $A(t) = \mathcal{R}_{A_\tau}(V(t))$  for some  $V$  in the tangent space at  $A_\tau$  that is evolved in time. Given  $Z_\tau$ , the problem reads

$$\begin{cases} \dot{V}(t) = f_\tau(V(t), Z^*(t)) & t \in \mathcal{T}_\tau, \\ \dot{Z}(t) = g_\tau^{\text{hROM}}(V(t), Z(t), U_\tau, P_\tau) & t \in \mathcal{T}_\tau, \\ V(t^\tau) = 0 \quad Z(t^\tau) = Z_\tau, \end{cases} \quad (25)$$

where  $f_\tau$  is defined as  $f_\tau = (d\mathcal{R}_{A_\tau|_{V(t)}})^{-1}Y_A(\mathcal{R}_{A_\tau}(V(t)), Z(t))$  via the inverse tangent map and

$$g_\tau^{\text{hROM}}(V(t), Z(t), U_\tau, P_\tau) := J_{2n_\tau}\nabla\mathcal{H}_\tau^{\text{hROM}}(\mathcal{R}_{A_\tau}(V(t))Z(t)).$$

Once  $V_{\tau+1}$  has been computed, the reduced basis at time  $t^{\tau+1}$  is obtained as  $A_{\tau+1} = \mathcal{R}_{A_\tau}(V_{\tau+1})$ .

Since  $U_\tau$  and  $P_\tau$  are fixed, system (25) can be solved using the 2-stage second order partitioned RK scheme introduced in [17, Lemma A.1], where the equation for  $V$  is solved using the explicit midpoint scheme and the equation for  $Z$  using the implicit midpoint rule. The application of the method to the hyper-reduced model (24) is presented in Algorithm 3. The initial reduced basis  $A_0$  can be obtained via complex SVD of the initial condition  $\mathcal{W}_0$ , while the initial coefficient matrix is defined as the projection of the initial condition onto the reduced space, that is,  $Z_0 := \mathcal{W}_0 - A_0 A_0^\top \mathcal{W}_0$ . We refer the reader to [25, 17] for further details regarding the derivation and properties of the temporal integrator.

---

### Algorithm 3 Partitioned RK2 scheme for the hyper-reduced model (24)

---

- 1: **procedure**  $(A_{\tau+1}, Z_{\tau+1}) = \text{PRK2\_HROM}(A_\tau, Z_\tau, Z_\tau^*, U_\tau, P_\tau)$
  - 2:  $\hat{k}_1^* = Y_A(A_\tau, Z_\tau^*)$
  - 3:  $k_2 = g_\tau^{\text{hROM}}\left(\frac{\Delta t}{2}\hat{k}_1^*, Z_\tau + \frac{\Delta t}{2}k_2, U_\tau, P_\tau\right)$
  - 4: Restrict  $k_2$  to the sample parameters:  $k_2^* := g_\tau^{\text{hROM}}\left(\frac{\Delta t}{2}\hat{k}_1^*, Z_\tau^* + \frac{\Delta t}{2}k_2^*, U_\tau, P_\tau\right)$
  - 5:  $\hat{k}_2 = f_\tau\left(\frac{\Delta t}{2}\hat{k}_1^*, Z_\tau^* + \frac{\Delta t}{2}k_2^*\right)$
  - 6:  $V_{\tau+1} \leftarrow \Delta t_\tau \hat{k}_2$  and  $A_{\tau+1} \leftarrow \mathcal{R}_{A_\tau}(V_{\tau+1})$
  - 7:  $Z_{\tau+1} \leftarrow Z_\tau + \Delta t_\tau k_2$
  - 8: **end procedure**
- 

## 7 Summary of the algorithm

The main steps of the proposed structure-preserving adaptive hyper-reduction method for the solution of the parametric system (2) are reported in Algorithm 4.

The computational complexity of Algorithm 4 is detailed below, where we report the highest possible computational cost for operations like the solution of a linear system, matrix-matrix multiplication,

---

**Algorithm 4** Structure-preserving adaptive hyper-reduction
 

---

```

1: procedure SPA-HYPER( $\mathcal{W}_0, K, N_t, \tau_{m_0}$ )
2:   Compute  $A_0$  via complex truncated SVD of  $\mathcal{W}_0$ 
3:    $Z_0 \leftarrow A_0^\top \mathcal{W}_0$ 
4:    $\lambda \leftarrow 0$ 
5:   Compute  $U_0$  via truncated SVD of  $D_h(A_0 Z_0) A_0$  with tolerance  $\tau_m$ 
6:    $P_0 \leftarrow \text{QDEIM}(U_0)$ 
7:   for  $\tau = 0, \dots, N_t - 1$  do
8:     Form  $\eta_\tau^*$  by selecting  $p_A^*$  parameters via pivoted QR of  $Z_\tau$ 
9:     Evaluate the error indicator  $e_\tau^*$  from  $W_\tau^* = A_\tau Z_\tau^*$ 
10:    if  $\tau = 0$  then
11:       $\bar{e} \leftarrow e_\tau^*$ 
12:    else if  $\tau > 0$  and  $e_\tau^* > \bar{e}K(\lambda)$  then
13:       $(A_\tau, Z_\tau, U_\tau, P_\tau) = \text{RANK\_UPDATE}(A_\tau, Z_\tau, Z_\tau^*, \tau_m)$  as in Algorithm 2
14:       $\bar{e} \leftarrow e_\tau^*, \lambda \leftarrow \lambda + 1$ 
15:      Form  $Z_\tau^*$  with the columns of  $Z_\tau$  associated with the parameters  $\eta_\tau^*$ 
16:    end if
17:     $(A_{\tau+1}, Z_{\tau+1}) = \text{PRK2\_HROM}(A_\tau, Z_\tau, Z_\tau^*, U_\tau, P_\tau)$  as in Algorithm 3
18:     $(U_{\tau+1}, P_{\tau+1}) = \text{EIM\_UPD}(A_{\tau+1}, Z_{\tau+1}, U_\tau, P_\tau, \tau_{m_s})$  as in Algorithm 1
19:  end for
20: end procedure

```

---

etc. These operations can be clearly accelerated in situations where the problem at hand has particular structures and sparsity patterns.

The computation of the initial data (lines 2-6) requires  $O(Npn_0) + O(pdm_0n_0) + O(dm_0^2)$  operations. Then, at each time step, Algorithm 4 incurs the following costs:

- $O(pp_A^*n_\tau)$  for the pivoted QR of  $Z_\tau$ .
- $O(Np_A^*n_\tau)$  for the evaluation of the error indicator  $e_\tau^*$
- $O(Nn_\tau^2) + O(Np_A^*n_\tau) + O(pn_\tau^3n_{\text{NL}}) + O(pn_\tau smn_{\text{NL}})$  for Algorithm 3, where  $n_{\text{NL}}$  is the number of iterations of the non-linear solver. More in details, the evaluation of the velocity  $Y_A$  at  $p_A^*$  sample parameters has leading complexity  $O(Nn_\tau^2) + O(Nn_\tau p_A^*)$  [17, Section 6]. Next, in the evaluation of  $\nabla \mathcal{H}_\tau^{\text{hROM}}(A, Z)$ , the vector  $(U_\tau^\top P_\tau)^{-1} U_\tau^\top v$  can be computed with  $O(m^3) + O(Nm)$  operations, and the evaluation of  $D_h$  at the  $m$  rows corresponding to the EIM interpolation indices  $P_\tau$  requires  $O(msn_\tau)$  operations, assuming that the cost of computing each entry of  $D_h$  is constant. Since each row of  $P_\tau^\top D_h$  only has  $s$  non-zero elements, the product with  $A_\tau$  requires  $O(msn_\tau)$  operations. Since  $s$  is also the number of non-zero entries in each row of  $\nabla^2 \mathcal{H}_\tau^{\text{hROM}}$ , the hyper-reduced Hessian can also be evaluated with  $O(msn_\tau)$  operations. For the computation of  $g_\tau^{\text{hROM}}$  a nonlinear system has to be solved for each of the  $p$  columns of  $k_2$ : if Newton's method is employed, each iteration consists of evaluating  $\nabla^2 \mathcal{H}_\tau^{\text{hROM}}$  and solving a  $2n_\tau \times 2n_\tau$  system for all test parameters. Thus,  $k_2$  is computed with complexity  $O(msn_\tau pn_{\text{NL}}) + O(n_\tau^3 pn_{\text{NL}})$ . Finally, with the algorithm proposed in [25, Section 5.3.1], the computation of the retraction  $\mathcal{R}_{A_\tau}$ , its inverse tangent map and the assembly of the operator  $f_\tau$  have arithmetic complexity  $O(Nn_\tau^2)$ .
- $O(Np_U^*n_\tau) + O(dp_U^*n_\tau r_C) + O(dm^2) + O(pp_U^*n_\tau) + O(pn_\tau mm_s)$  for Algorithm 1 as derived in Section 3.2.

In addition, at each rank update, Algorithm 2 is applied with arithmetic complexity  $O(N(p_A^*)^2) + O(dn_{\tau+1}sp_A^*) + O(dp_A^*n_{\tau+1}m) + O(dm^2)$ . Indeed, computing the SVD of the projection error at most  $E_P(\mathcal{W}^*) \in \mathbb{R}^{2N \times p_A^*}$  requires  $O(N(p_A^*)^2)$  operations, while the complexities of assembling the snapshot matrix  $D(A^{\text{new}}, (Z^{\text{new}})^*)$  and computing its truncated SVD with tolerance  $\tau_m$  are  $O(dn_{\tau+1}sp_A^*)$  and  $O(dn_{\tau+1}p_A^*m)$ , respectively. Finally, the new DEIM interpolation indices are recomputed via QDEIM with complexity  $O(dm^2)$ . Note that the matrix-matrix multiplications involved in the definition of  $Z^{\text{new}}$  can be avoided since it can be easily seen that  $Z^{\text{new}}$  is obtained by augmenting  $Z$  with  $n_{\tau+1} - n_\tau$  rows of zeros.

A reduction in the computational runtimes of the algorithm compared to the solution of the reduced dynamics (6) is thus achieved by decoupling the operations that depend on the dimension of the full order model from those that depend on the number of parameters.

## 8 Numerical experiments

In the two-dimensional, rectangular domain  $\Omega = [-L_x, L_x] \times [-L_y, L_y] \subset \mathbb{R}^2$ , we consider the nonlinear Schrödinger equation

$$\begin{cases} i \frac{\partial u}{\partial t} + \Delta u + \gamma |u|^2 u = 0 & \text{in } \Omega \times \mathcal{T}, \\ u(0, x, y; \alpha, \beta) = u^0(x, y; \alpha, \beta) & \text{in } \Omega, \end{cases} \quad (26)$$

with periodic boundary conditions. The solution depends on the parameter vector  $\eta = (\alpha, \beta, \gamma) \in \Gamma \subset \mathbb{R}^3$ , where  $\gamma$  enters the equation, while  $\alpha$  and  $\beta$  enter the initial condition. The Hamiltonian formulation of this problem is obtained by writing  $u(t, x, y; \eta) = q(t, x, y; \eta) + ip(t, x, y; \eta)$  and deriving evolution equations for the real and imaginary parts,  $q$  and  $p$  respectively:

$$\begin{cases} \frac{\partial q}{\partial t} = -\Delta p - \gamma(q^2 + p^2)p & \text{in } \Omega \times \mathcal{T}, \\ \frac{\partial p}{\partial t} = \Delta q + \gamma(q^2 + p^2)q & \text{in } \Omega \times \mathcal{T}. \end{cases} \quad (27)$$

This is a Hamiltonian system with Hamiltonian given by

$$\frac{1}{2} \int_{\Omega} \left( |\nabla q|^2 + |\nabla p|^2 - \frac{\gamma}{2}(q^2 + p^2)^2 \right) dx dy.$$

Problem (27) is discretized in space using a second-order finite difference scheme on a uniform grid with  $N_x$  and  $N_y$  intervals in the  $x$  and  $y$  direction, respectively. Namely, we define the grid points  $x_i := -L_x + i\Delta x$  for  $i = 1, \dots, N_x$  and  $y_j := -L_y + j\Delta y$  for  $j = 1, \dots, N_y$ , with  $\Delta x = 2L_x/N_x$  and  $\Delta y = 2L_y/N_y$ . The dimension of the full order problem is then  $2N$  with  $N := N_x N_y$ . We denote by  $q_{i,j}$  and  $p_{i,j}$  the approximations to  $q(x_i, y_j)$  and  $p(x_i, y_j)$ , respectively, for  $i = 1, \dots, N_x$  and  $j = 1, \dots, N_y$ . The full order state  $w$  is defined as  $w = (q_h^\top, p_h^\top)^\top \in \mathbb{R}^{2N}$ , with

$$\begin{aligned} q_h &:= (q_{1,1}, \dots, q_{N_x,1}, q_{1,2}, \dots, q_{N_x,2}, \dots, q_{1,N_y}, \dots, q_{N_x,N_y})^\top \in \mathbb{R}^N, \\ p_h &:= (p_{1,1}, \dots, p_{N_x,1}, p_{1,2}, \dots, p_{N_x,2}, \dots, p_{1,N_y}, \dots, p_{N_x,N_y})^\top \in \mathbb{R}^N. \end{aligned}$$

Then the full order system reads

$$\dot{w} = \begin{pmatrix} \dot{q}_h \\ \dot{p}_h \end{pmatrix} = J_{2N} \begin{pmatrix} -\mathbb{D}q_h - \gamma(q_h^2 + p_h^2) \odot q_h \\ -\mathbb{D}p_h - \gamma(q_h^2 + p_h^2) \odot p_h \end{pmatrix} = J_{2N} \nabla_w \mathcal{H}_\eta(w),$$

where  $\mathbb{D} \in \mathbb{R}^{N \times N}$  is the discrete Laplacian matrix,  $\odot$  denotes the component-wise product of vectors,  $q_h^2 := q_h \odot q_h$  and  $\mathcal{H}_\eta$  is the discrete Hamiltonian defined as

$$\mathcal{H}_\eta(w) := \frac{1}{2} \left( -q_h^\top \mathbb{D} q_h - p_h^\top \mathbb{D} p_h - \frac{\gamma}{2} \sum_{i=1}^{N_x} \sum_{j=1}^{N_y} (q_{i,j}^2 + p_{i,j}^2)^2 \right). \quad (28)$$

Following the procedure described in Section 3, we decompose the non-quadratic part of the Hamiltonian (28) as  $\mathcal{H}_\eta(w) = v^\top h(w)$  where  $v$  is the vector of  $\mathbb{R}^N$  whose entries are all 1 and

$$h(w) := -\frac{\gamma}{4} (q_h^2 + p_h^2)^2 \in \mathbb{R}^N.$$

Note that in this case we have  $d = N$ , and each entry of  $h$  only depends on two components of the state  $w$ . Therefore, the Jacobian matrix of  $h$  is the concatenation of two  $N \times N$  diagonal matrices, namely

$$D_h(w) = -\gamma \left[ \text{diag}(q_h \odot (q_h^2 + p_h^2)) \quad \text{diag}(p_h \odot (q_h^2 + p_h^2)) \right] \in \mathbb{R}^{N \times 2N},$$

where  $\text{diag}$  denotes a diagonal matrix.

In the numerical experiments we set  $L_x = L_y = 2\pi$  and  $N_x = N_y = 100$ , so that the full system has dimension  $2N = 2N_x N_y = 20000$ . The final time is  $T = 3$  and we consider  $N_t = 12000$  uniform temporal intervals so that  $\Delta t = 2.5 \times 10^{-4}$ . Note that the choice of such a relatively small time step is not dictated by stability issues but only to facilitate the study of the approximation error associated with the reduction and hyper-reduction without pollution from the temporal integration error. The full order system is solved using the implicit midpoint rule, while the reduced and hyper-reduced systems are solved using the partitioned RK scheme described in Section 6. Since the proposed time integrators are (semi-)implicit, a nonlinear system has to be solved for each test parameter at each time step: the Newton

method with stopping tolerance  $\tau = 10^{-10}$  is chosen as nonlinear solver. This operation is parallelized in the numerical solution of the full and reduced system using 16 cores while no parallelization is performed on the hyper-reduced system. In fact, in the latter case the runtime to solve the resulting nonlinear system is so small that no computational gain is achieved by parallelizing the computation because of overhead costs. For the sake of a fair comparison, the computational time per core per test parameter is taken as a unit of measure, in the sense that the computational time required by each operation is multiplied by the number of cores on which the operation is executed.

Finally, in all numerical experiments, we assess the accuracy of the different algorithms in terms of relative errors in the Frobenius norm with respect to the full order solution, namely

$$\mathcal{E}(t) := \frac{\|\mathcal{W}(t) - W(t)\|_F}{\|\mathcal{W}(t)\|_F}$$

where  $W$  can be the numerical solution of the reduced system (6) or of the hyper-reduced system (24).

## 8.1 Test 1: Localized solution

In the first scenario, we consider as initial condition of problem (26) a hump placed at the center of the computational domain  $\Omega$ , namely

$$u^0(x, y; \alpha, \beta) = \frac{\sqrt{2}}{\cosh(\alpha x) \cosh(\beta y)} \exp\left(i\frac{x}{2}\right) \exp\left(i\frac{y}{2}\right). \quad (29)$$

The parameter set for this problem is  $\Gamma = [0.8, 2] \times [0.8, 2] \times [-1.5, -0.5]$ ; the set of test parameters is obtained by discretizing  $\Gamma$  with 5 uniformly spaced parameters in each direction, so that  $p = 5^3 = 125$ . Figure 1 shows the numerical solution corresponding to two different test parameters. The time required to solve the full order system is 5241 s per core per test parameter. The growth of the numerical rank of the

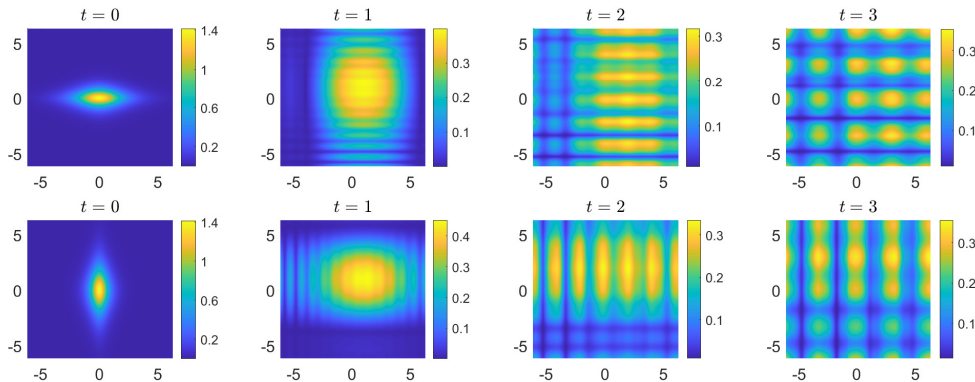


Figure 1: Test 1, localized initial condition. Numerical solution of the full order problem at four different time instants. First row  $\eta = (0.8, 2, -1.5)$ ; second row  $\eta = (2, 0.8, -0.5)$ .

full solution, for different values of the threshold  $\epsilon$ , is shown in Figure 2. This test case is characterized by a growth of the numerical rank in the first stages of the simulation. We expect the error in the non-adaptive reduced and hyper-reduced systems to possess a similar behavior, while the rank-adaptive strategy should correctly capture this evolution and keep the error constant over time.

### 8.1.1 Non-rank-adaptive algorithm

In a first test, we assess the capability of the hyper-reduction strategy to reduce the computational cost of the reduced system while achieving a comparable error. To this end, we consider the non-rank-adaptive case by fixing the dimension of the reduced space, i.e.,  $n_\tau = n_0$  for  $\tau = 1, \dots, N_t$ . The hyper-reduced system is solved using the adaptive strategy described in Section 3.1. In particular, the EIM adaption is performed at each time step with  $\tau_{m_s} = 10^{-4}$ . First, we set  $2n_0 = 24$ . The error of the reduced system is shown in Figure 3, left (dashed line): the relative error is below  $10^{-3}$  at the initial time, then increases rapidly at the beginning of the simulation, while the growth becomes less evident starting from about  $t = 0.5$ , which reflects the behavior of the numerical rank of the full solution, see Figure 2. Concerning the hyper-reduced system, we determine the dimension of the EIM space by performing POD on the nonlinear term at the initial time with tolerance  $\tau_m = 10^{-8}$ , which results in  $m_\tau = m_0 = 80$ . The relative error of the hyper-reduced system is shown in Figure 3 (left) for different choices of  $p_A^*$  and  $p_U^*$ , whose evolution is reported in Figure 3 (right). Table 1 reports the computational times and the relative errors

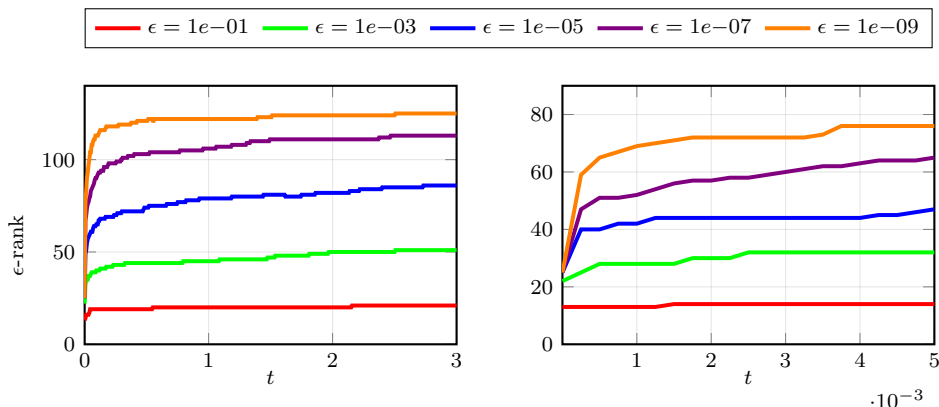


Figure 2: Test 1, localized initial condition.  $\epsilon$ -rank of the full solution  $\mathcal{W}(t) \in \mathbb{R}^{20000 \times 125}$  for  $t \in [0, T]$  (left) and a zoom on the first 20 time steps,  $t \in [0, 20\Delta t]$  (right).

at the final time. In all cases considered, the computational times are reduced by at least a factor 13 compared to the reduced system with an almost negligible effect on the relative error. Moreover, the hyper-reduced system with  $p_A^* < p$  and  $p_U^* < p$  is solved in about half of the time required to perform the same task with  $p_A^* = p_U^* = p$ . In this case, the hyper-reduced system is about 25 times cheaper than the reduced system.

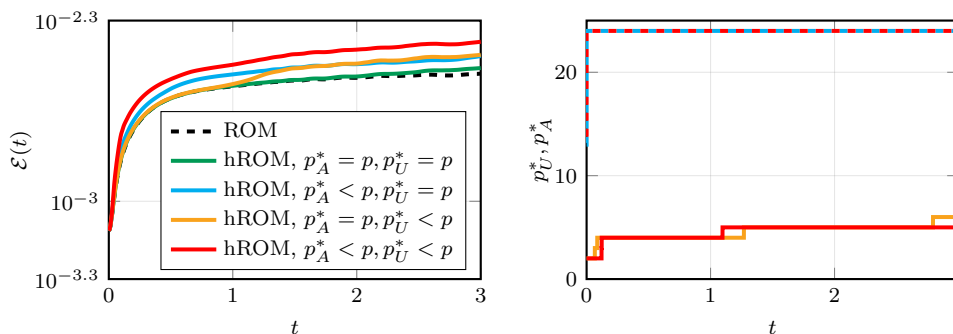


Figure 3: Test 1, localized initial condition. Dimension of the dynamical reduced basis space  $2n_\tau = 2n_0 = 24$ . Left: relative errors of the hyper-reduced system over time for  $m_\tau = m_0 = 80$  and with different choices of the sample parameters. The dashed black line represents the relative error of the reduced system. Right:  $p_U^*$  (solid lines) and  $p_A^*$  (dashed lines).

Table 1: Test 1, localized initial condition. Non-adaptive case,  $2n_\tau = 2n_0 = 24$ ,  $m = 80$ . Computational times and relative errors at the final time.

Model	Runtime [s]	Relative error at the final time
ROM	675.7	3.1168e-03
hROM, $p_A^* = p, p_U^* = p$	50.5	3.2763e-03
hROM, $p_A^* < p, p_U^* = p$	45.6	3.6444e-03
hROM, $p_A^* = p, p_U^* < p$	34.0	3.6870e-03
hROM, $p_A^* < p, p_U^* < p$	27.5	4.1408e-03

In this experiment, the use of a small number  $p_U^*$  of sample parameters in the context of EIM adaptivity leads to a considerable gain in terms of computational efficiency. In particular, the quantity  $\delta$  defined in Section 3.1 can be evaluated cheaply. This is related to the number of EIM sample indices  $m_s$  selected for the basis update. Figure 4 shows the evolution of this quantity over time: only about 1000 sample indices need to be selected when the tolerance is set to  $\tau_{m_s} = 10^{-4}$ , and this value is considerably smaller than the full dimension  $d = 10000$ . The behavior shown in Figure 4 is strictly related to the decay of local coherence of the EIM space. As noted in [27, Section 3.3], when a problem is characterized by moving coherent structures that are local in space, it is typically sufficient to adapt the EIM basis at a few sample indices only.

We repeat the tests presented above in the case  $2n_0 = 40$ . In principle, one may choose an even higher value of the reduced dimension, in order to approximate the initial condition with arbitrary accuracy: in this case, since it is known from Figure 2 that the initial condition has exact rank 25, setting  $2n_0 = 50$  would exactly capture the rank of the full solution at the initial time. Nevertheless, it is reasonable to pick the dimension of the initial reduced space in such a way that the low-rank approximation error is comparable to the error introduced by the temporal approximation. Numerical experiments (not shown here) show that the latter is around  $10^{-5}$  with the current choice of the temporal scheme and time step  $\Delta t$ .



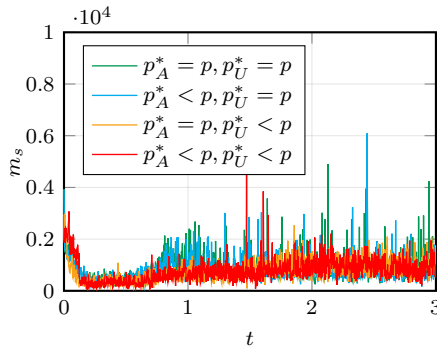


Figure 4: Test 1, localized initial condition. Evolution of the number  $m_s$  of EIM sample indices selected according to Algorithm 1 with  $\tau_{m_s} = 10^{-4}$ .

Therefore, we set  $2n_0 = 40$  since this choice yields a relative approximation error of the initial condition just above  $10^{-5}$ . The hyper-reduced system is solved in the non-rank-adaptive case with  $m_\tau = m_0 = 115$ . The EIM basis is adapted at every time step with  $\tau_{m_s} = 10^{-4}$ . Relative errors in the non-rank-adaptive case are plotted in Figure 5.

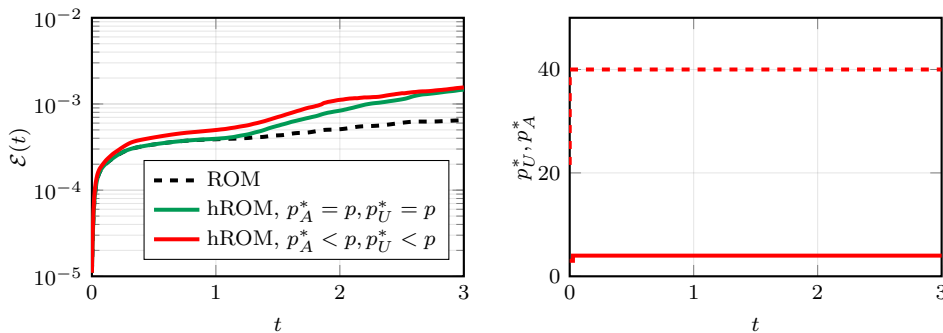


Figure 5: Test 1, localized initial condition. Dimension of the dynamical reduced basis space  $2n_\tau = 2n_0 = 40$ . Left: relative errors of the hyper-reduced system over time for  $m_\tau = m_0 = 115$  and with different choices of the sample parameters. The dashed black line represents the relative error of the reduced system. Right:  $p_U^*$  (solid line) and  $p_A^*$  (dashed line).

Table 2: Test 1, localized initial condition. Non-adaptive case,  $2n_\tau = 2n_0 = 40$ ,  $m = 115$ . Computational times and relative errors at the final time.

Model	Runtime [s]	Relative error at the final time
ROM	1360.7	6.5029e-04
hROM, $p_A^* = p, p_U^* = p$	99.5	1.4678e-03
hROM, $p_A^* < p, p_U^* < p$	38.0	1.5591e-03

A similar behavior to the test with  $2n_\tau = 24$  is observed, in the sense that the error exhibits a rapid growth in the first time instants. On the other hand, the error of the hyper-reduced system remains comparable to that of the reduced system only until about  $t = 1$ . We suspect that this is due to the fact that, even in the non-rank-adaptive case, the dimension of the EIM space should be increased to account for changes in the behavior of the numerical solution. This observation is motivated by Figure 1, which shows that the solution loses its localized structure starting from  $t > 1$ . In other words, while the choice  $m = 115$  provides an accurate approximation of the nonlinear term at the initial time, it may no longer be the case as the dynamics becomes more complex. We will show in the next section that the rank-adaptive strategy can overcome this issue, as the dimension of the EIM basis is also modified after the rank update. In terms of computational efficiency, Table 2 shows that the hyper-reduced system is about 14 times faster than the reduced system. Note that this value is comparable to that obtained in the case  $2n_\tau = 24$ . Moreover, when  $p_A^*$  and  $p_U^*$  sample parameters are used, the hyper-reduced system is over 2.5 times faster, with a negligible effect on the error. In fact, as shown in Figure 5, we have  $p_U^* = 4 \ll p$  for almost the entire simulation.

### 8.1.2 Rank-adaptive algorithm

In a second test we consider again the initial condition (29) and we numerically show how the rank-adaptive strategy of Section 4 can be used to overcome the growth of the approximation errors introduced by the reduction. In particular, the rank-adaptive algorithm uses the error indicator  $r$  defined in (21) and

computed at every time step. For the update criterion we set  $C_1 = C_2 = 1.1$ . Several other numerical tests (not reported here) show that the choice of these parameters has little impact on the quality of the approximation (see also [17]). Whenever the dimension  $2n_\tau$  of the reduced basis space is updated, the EIM dimension  $m$  is modified accordingly as in Algorithm 2, that is, an SVD is performed on the snapshots of the reduced Jacobian associated to the new reduced basis and coefficients with tolerance  $\tau_m = 10^{-4}$ . The initial value of  $m$  is also determined based on the same tolerance, which gives  $m_0 = 38$ . Finally, we consider  $p_A^* < p$  and  $p_U^* < p$  sample parameters to solve the hyper-reduced system with rank adaptivity. Figure 6 (left) shows the evolution of the relative errors in the reduced and hyper-reduced system, and the comparison with the same quantities without rank adaptivity (indicated with “NRA” in the legend). We also report the evolution of the values of the reduced dimension  $2n_\tau$  (central plot) and of the EIM dimension  $m_\tau$  (right plot). In this test the initial dimension of the reduced space is set to  $2n_0 = 24$ .

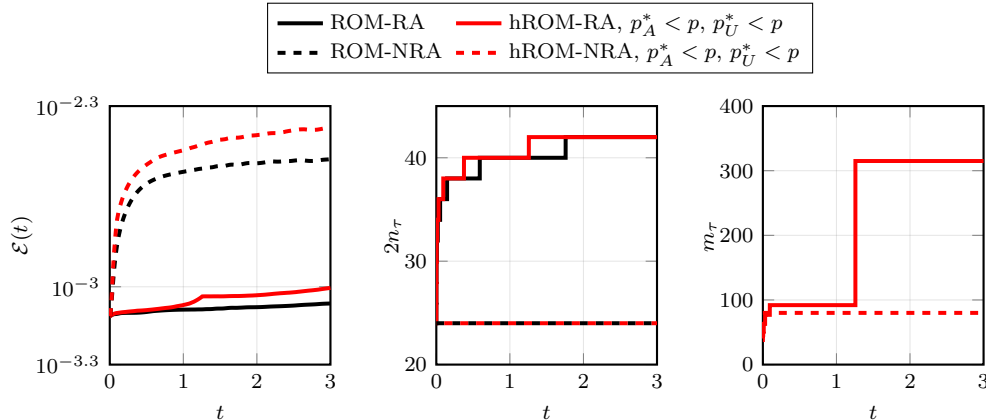


Figure 6: Test 1, localized initial condition. Rank-adaptive case,  $2n_0 = 24$ ,  $\tau_m = \tau_{m_s} = 10^{-4}$ . Left: evolution of the relative errors of the reduced and the hyper-reduced systems. Center: evolution of the dimension  $n_\tau$  of the reduced space. Right: evolution of the dimension  $m$  of the EIM space.

We observe that the value of  $2n_\tau$  is adapted frequently in the early stages of the simulation, while the update frequency decreases sensibly as time evolves. In this sense, our adaptive strategy is able to correctly capture the behavior of the numerical rank of the full solution reported in Figure 2. Similarly, we observe a variation of the EIM dimension  $m_\tau$ . Although the dimension of the EIM space is above 300 at the final time, this value is still about 3% of the full dimension  $d = N$ , and this is sufficient to yield a computational gain compared to the reduced system, as it can be inferred from the data reported in Table 3. The rank-adaptive algorithm for the hyper-reduced system is about 17 times faster than the rank-adaptive algorithm applied to the reduced system, for the same value of  $n_0$ . Moreover, when compared to the reduced system without rank adaptivity, the rank-adaptive hyper-reduced system yields a relative error at the final time that is over 3 times smaller, with a reduction by a factor 6 in the computational time.

Table 3: Test 1, localized initial condition. Rank-adaptive case,  $2n_0 = 24$ ,  $\tau_m = \tau_{m_s} = 10^{-4}$ . Computational times and relative errors at the final time.

Model	Runtime [s]	Relative error at the final time
ROM-RA	1984.0	8.6167e-04
hROM-RA	116.4	9.8997e-04
ROM-NRA	675.7	3.1168e-03
hROM-NRA	27.5	4.1408e-03

Finally, we present in Figure 7 the time evolution of the error indicator  $r$ , and a comparison with the angle  $\theta$  from [6] and defined in (20). The latter fails to identify the increase in the rank of the solution: its value never satisfies the update criterion so that no rank update is performed at all. On the other hand, the error indicator based on the residual  $r$ , which is related to  $\theta$  but also takes into account its time evolution, is able to reflect the behavior of the rank of the solution.

Finally, we test the rank-adaptive scheme with  $2n_0 = 40$ . The parameters in the update criterion are  $C_1 = 1.2$ ,  $C_2 = 1.1$ . In the hyper-reduced system, the EIM space is updated at each time step with  $\tau_{m_s} = 10^{-6}$ , while the EIM basis is recomputed after each rank update with  $\tau_m = 10^{-6}$ . Notice that this value is taken two orders of magnitude smaller compared to the case  $2n_0 = 24$  to account for the increased accuracy in the approximation given by the reduced basis. Figure 8 shows the results and a comparison with the non-rank-adaptive case, while computational times are reported in Table 4.

For the rank-adaptive algorithm, hyper-reduction has the effect of reducing the computational time by

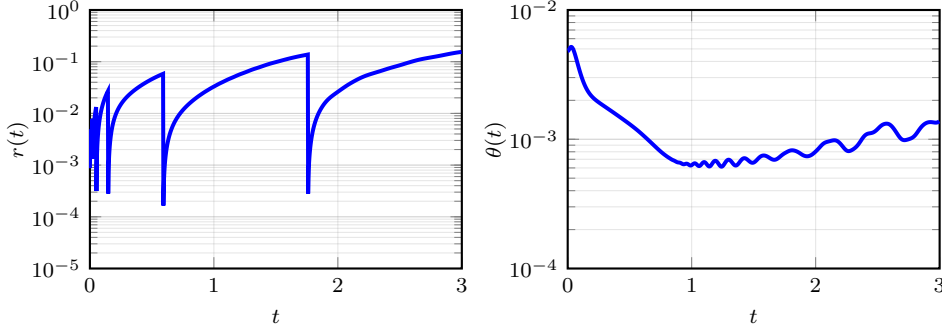


Figure 7: Test 1, localized initial condition. Time evolution of the error indicators  $r$  and  $\theta$ .

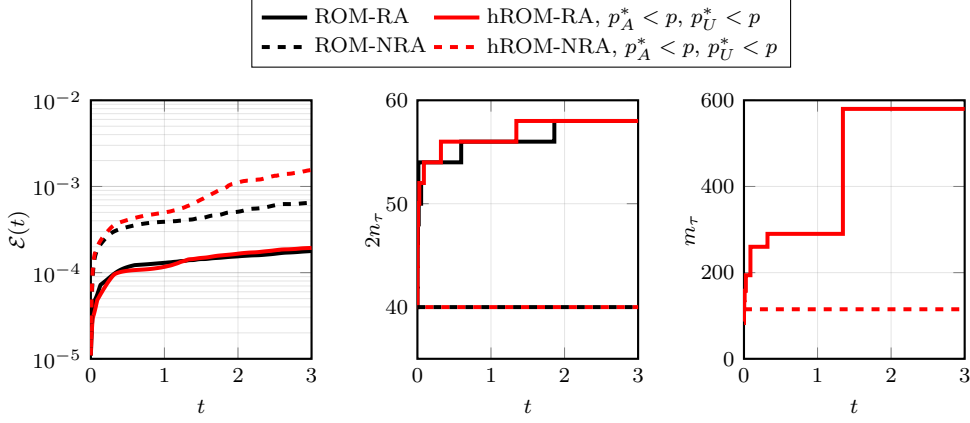


Figure 8: Test 1, localized initial condition. Rank-adaptive case,  $2n_0 = 40$ ,  $\tau_m = \tau_{m_s} = 10^{-6}$ . Left: evolution of the relative errors of the reduced and the hyper-reduced systems. Center: evolution of the dimension  $n_\tau$  of the reduced space. Right: evolution of the dimension  $m$  of the EIM space.

a factor 4 with respect to the reduced system, with a comparable error at the final time. Even compared to the non-rank-adaptive reduced system, rank-adaptivity combined with hyper-reduction yields a relative error over 3 times smaller at the final time in about a third of the total computational time. Moreover, as anticipated, the hyper-reduced error reproduces the behavior of the reduced error as the dimension of the EIM space is also updated.

Notice that the tolerances  $\tau_m$  and  $\tau_{m_s}$  and the EIM update frequency  $\Delta$  have been kept fixed in these experiments. On the other hand, it is reasonable to assume that, as  $m$  increases, one may afford a larger value  $\Delta$  and, hence, the computational gain in the hyper-reduced system might be improved when adaptive strategies to select  $\Delta$  and  $\tau_m$  are implemented. A rigorous development of this strategy is left for future work. Here we implement a preliminary test, where the value of  $\tau_m$  is modified during the online phase. In particular, we fix  $\tau_{m_s} = 10^{-6}$  while we set  $\tau_m = 10^{-6}$  for  $t \leq 0.5$  and  $\tau_m = 10^{-4}$  for  $t > 0.5$ . The threshold  $t = 0.5$  is determined *a posteriori* from the behavior of the relative error over time displayed in Figure 8. With this choice, the computational time is reduced by almost 50% compared to the case of fixed  $\tau_m$ , with a comparable error at the final time (see Table 5). This example shows the advantages of an adaptive strategy for the selection of the tolerance  $\tau_m$ .

To summarize, Figure 9 shows the errors at the final time as a function of the computational time in the experiments discussed above.

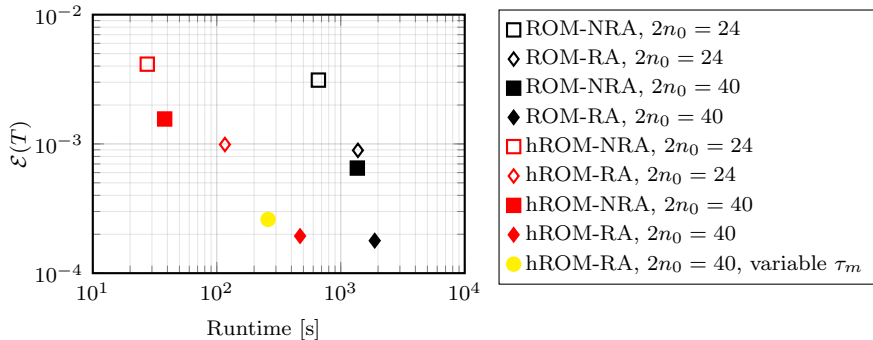


Figure 9: Test 1, localized initial condition. Rank-adaptive case. Relative errors at the final time vs. computational time.

Table 4: Test 1, localized initial condition. Rank-adaptive case,  $2n_0 = 40$ ,  $\tau_m = \tau_{m_s} = 10^{-6}$ . Computational times and relative errors at the final time.

Model	Runtime [s]	Relative error at the final time
ROM-RA	1879.8	1.7845e-04
hROM-RA	469.9	1.9378e-04
ROM-NRA	1360.7	6.5029e-04
hROM-NRA	38.0	1.5591e-03

Table 5: Test 1, localized initial condition. Rank-adaptive case,  $2n_{\tau_0} = 40$ ,  $\tau_{m_s} = 10^{-6}$ . Computational times and relative errors at the final time of the hyper-reduced system. Fixed  $\tau_m$  vs. variable  $\tau_m$ .

$\tau_m$	Runtime [s]	Relative error at the final time
Fixed	469.9	1.9378e-04
Variable	259.4	2.6057e-04

A few observations can be made. First, all red markers are to the left of the corresponding black markers meaning that hyper-reduction allows a reduced computational time to achieve comparable errors at the final time, both in the non-rank-adaptive and in the rank-adaptive case.

Moreover, diamond-shaped markers (rank-adaptive algorithms) are below and to the right of the corresponding square-shaped markers (non-rank-adaptive algorithms), meaning that the errors obtained with rank adaptivity are smaller than those obtained in the non-rank-adaptive cases, at the cost of a slightly increased algorithm runtime. The runtime growth is more evident in the hyper-reduced system when the dimension of the reduced space is large, because the EIM space dimension  $m$  is also enlarged due to rank adaptation. Nevertheless, efficiency can be improved in these cases by an adaptive selection of the tolerance  $\tau_m$  and/or of the update frequency  $\Delta$  (circle mark in Figure 9). The accuracy of the rank-adaptive hyper-reduced model is not achievable by the non-rank-adaptive algorithms since it would require to select a rank of the initial approximate state larger than the actual rank of the initial full state leading to over-approximation of the dynamics at the initial time, ill-conditioned systems and no runtime gain.

For the reduced order model, we observe that the rank-adaptive reduced system with  $2n_0 = 24$  (black empty diamond) is as computationally expensive as the non-rank-adaptive reduced system with  $2n_0 = 40$  (black full square), with a slightly larger error at the final time. This is due to the fact that, as shown in Figure 6 (center), the dimension of the reduced space in the rank-adaptive case increases rapidly at the beginning of the simulation, reaching the value  $2n_\tau = 40$  at about  $t = 0.5$  in agreement with the rapid growth of the numerical rank of the full solution that characterizes this test case (see Figure 2). Therefore, the reduced space in the rank-adaptive case is considerably smaller than in the non-adaptive case only in the first few time steps, which explains the similar runtimes of the two schemes. Moreover, the error in the rank-adaptive case is determined by the choice of the initial reduced dimension  $2n_0$ . Since the error in the non-adaptive case does not exhibit a significant growth at later stages of the simulation, its value at the final time is smaller than the one obtained with rank adaptivity and a smaller initial reduced space. Although this represents a possible case scenario, we expect, in general, the rank-adaptive (hyper-)reduced system to outperform its non-rank-adaptive counterpart with a larger initial reduced space in all situation where the rank of the full order solution undergoes significant changes over time.

## 8.2 Test 2: Non-localized solution

In a second test, we consider the following initial condition [17]

$$u^0(x, y; \alpha, \beta) = (1 + \alpha \sin x)(2 + \beta \sin y).$$

We fix  $\gamma = -1$  in equation (26) so that the parameter vector is  $\eta = (\alpha, \beta)$  and we take  $\Gamma = [0.97, 1.03] \times [0.97, 1.03] \subset \mathbb{R}^2$  as parameter set. We solve (26) for  $p = 100$  test parameters obtained by sampling  $\Gamma$  with 10 equispaced parameters in each direction. The quantities involved in the spatial and temporal discretizations are the same as in the previous test. In particular, the full system has dimension  $2N = 20000$  and it is solved for  $N_t = 12000$  time steps until the final time  $T = 3$ , which requires about 6257.7 s. The numerical solution is shown in Figure 10 for two test parameters. We observe that, unlike in the previous case, this problem is not characterized by coherent structures that are local in space, except for the initial stages of the simulation. Figure 11 shows the growth of the numerical rank of the full solution. The main difference with respect to the previous test case (see Figure 1) is that the numerical rank keeps increasing during the simulation, which makes it a challenging test.

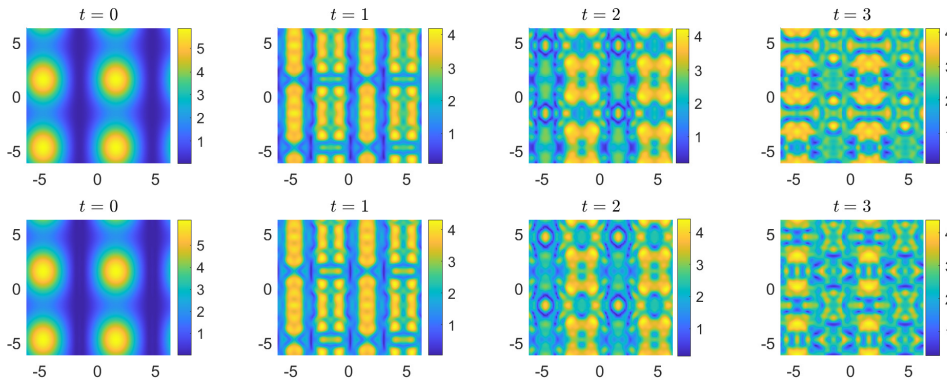


Figure 10: Test 2, non-localized solution. Numerical solution of the full order problem at four different time instants. First row  $\eta = (0.97, 0.97)$ ; second row  $\eta = (1.03, 1.03)$ .

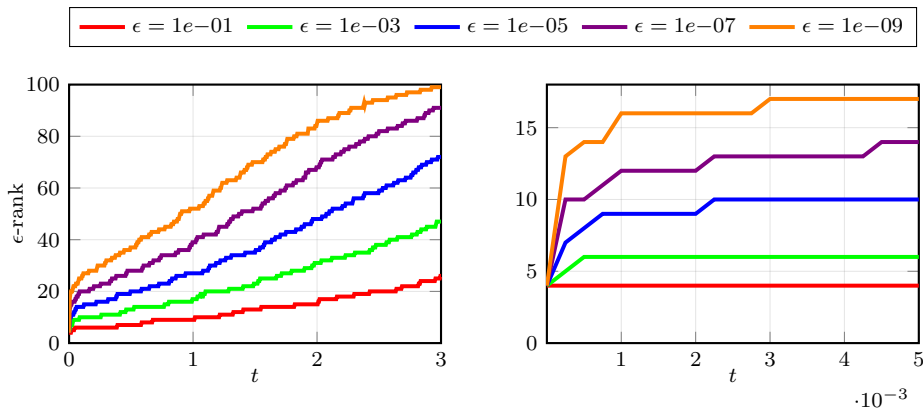


Figure 11: Test 2, non-localized solution.  $\epsilon$ -rank of the full solution  $\mathcal{W}(t) \in \mathbb{R}^{20000 \times 100}$  for  $t \in [0, T]$  (left) and a zoom on the first 20 time steps,  $t \in [0, 20\Delta t]$  (right).

### 8.2.1 Non-rank-adaptive algorithm

First, we assess the performances of the reduced and hyper-reduced systems when the dimension of the reduced space is not updated during the simulation. To this end, we fix  $2n_\tau = 2n_0 = 8$  which is the exact rank of the initial condition. The evolution of the relative errors with respect to the full order solution is shown in Figure 12 (left). Differently from the first test case, numerical errors increase at a constant rate until the final time, which is in accordance with the increase of the numerical rank of the full solution from Figure 11. In the hyper-reduced system, the initial EIM basis is constructed via POD of the snapshot matrix of the nonlinear reduced Jacobian with tolerance  $\tau_m = 10^{-10}$ , which yields  $m_0 = 25$ . The EIM update is then performed at every time step with  $\tau_{m_s} = 10^{-4}$ . We test different combinations of the choices of sample parameters  $p_A^*$  and  $p_U^*$ . The computational time required by the different algorithms is reported in Table 6.

In the best case scenario, we observe a reduction of the computational time by a factor 25 compared to the reduced order model. An important remark is that, in contrast with the localized case, updating the EIM basis using  $p_U^* < p$  sample parameters does not yield any computational gain; on the contrary, this choice turns out to be more expensive than performing the update with all  $p$  test parameters. The reason behind this behavior is related to the number  $m_s$  of sample EIM indices, which is shown in Figure 13. The non-local nature of the problem causes the value of  $m_s$  to be comparable to  $d = N$  for a large portion of the time window  $[0, T]$ . This is, in turn, related to the slow decay of the local coherence of the EIM space in the absence of propagating coherent structures. As shown in Section 3.1, the arithmetic complexity of selecting  $p_U^*$  sample indices and updating the EIM basis depends, among others, on the product of the number of test parameters  $p$  with the number of sample indices  $m_s$ , and this cost becomes dominant when  $m_s \approx d$ . In particular, the most expensive operation is the computation of  $\delta$ , which requires evaluating the nonlinear term at the EIM sample indices for all test parameters. Hence, using only  $p_U^*$  sample parameters to perform the EIM update does not compensate for this extra cost, not even when  $p_U^* \ll p$ . In view of this fact, we will set  $p_U^* = p$  in the following. On the other hand, a significant reduction of computational time can be seen when  $p_A^* < p$  sample parameters are used to evolve the reduced basis. This reduction amounts to over 30% when  $p_U^* = p$ . In all cases, there is little difference in the relative errors compared to the benchmark case  $p_U^* = p_A^* = p$ .

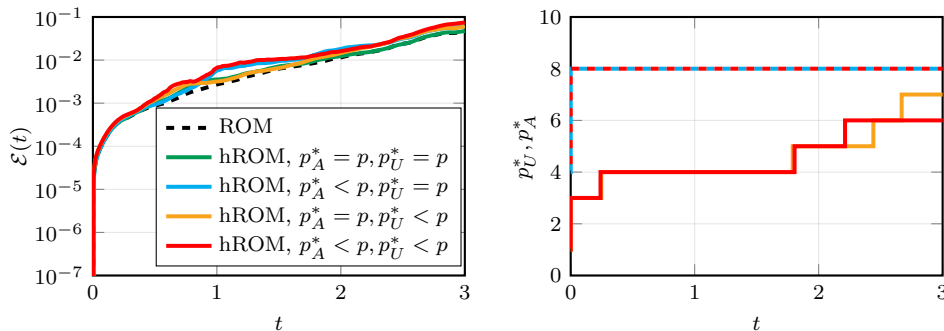


Figure 12: Test 2, non-localized solution. Dimension of the dynamical reduced basis space  $2n_\tau = 2n_0 = 8$ . Left: relative errors of the hyper-reduced system over time for  $m_\tau = m_0 = 25$  and with different choices of the sample parameters. The dashed black line represents the relative error of the reduced system. Right:  $p_U^*$  (solid lines) and  $p_A^*$  (dashed line).

Table 6: Test 2, non-localized solution. Non-adaptive case,  $2n_\tau = 2n_0 = 8$ ,  $m = 25$ . Computational times and relative errors at the final time.

Model	Runtime [s]	Relative error at the final time
ROM	375.7	4.6121e-02
hROM $p_A^* = p, p_U^* = p$	21.1	4.7334e-02
hROM $p_A^* < p, p_U^* = p$	14.8	5.9889e-02
hROM $p_A^* = p, p_U^* < p$	29.0	6.0908e-02
hROM $p_A^* < p, p_U^* < p$	23.2	7.4322e-02

### 8.2.2 Rank-adaptive algorithm

We now test the rank-adaptive strategy of Section 4 in order to mitigate the growth of the error due to the increasing rank of the full solution. We consider  $C_1 = C_2 = 1.1$  in the update criterion, and we compare the two error indicators described in Section 4. The dimension of the reduced space at the initial time is  $2n_0 = 8$  and a tolerance  $\tau_m = \{10^{-6}, 10^{-8}\}$  is used to adapt the dimension of the EIM space. The EIM sample indices are computed based on the tolerance  $\tau_{m_s} = 10^{-4}$ . On the basis of the previous experiments, we set  $p_U^* = p$  and  $p_A^* < p$  in the hyper-reduced system. Figure 14 (left) shows the time evolution of the relative error in the reduced and hyper-reduced systems, the evolution of the dimension  $2n_\tau$  of the reduced space (center) and the evolution of the dimension  $m_\tau$  of the EIM space (right), comparing  $r$  and  $\theta$  as error indicator for the rank adaptivity. The results are compared to the errors obtained in the reduced system with the same value of  $2n_0$  and no rank adaptivity.

When  $r$  is used as error indicator and  $\tau_m = 10^{-8}$ , the error of the rank-adaptive hyper-reduction algorithm is comparable to that of the reduced system. Moreover, we observe that the errors resulting from the rank-adaptive algorithms increase at a smaller rate than the error associated to the non-adaptive method. One may be interested in exploiting the rank-adaptive strategy to keep the value of the error approximately constant over time. One possibility to achieve this is to set the value of  $C_2$  equal to 1, so that the update frequency is not limited. Nevertheless, one should always keep in mind the interplay between accuracy and computational efficiency. Numerical tests not reported here show that the reduced space might become unnecessarily large without any control on the update frequency. In addition, other factors, such as the error of time integration, prevent the reduced and hyper-reduced errors from remaining flat.

In contrast with the case of a localized solution, this choice actually results in some updates of the reduced dimension. Nevertheless, these updates are not frequent enough to produce a significant improvement in the numerical errors. Compared to  $\theta$ , our indicator  $r$  allows for a better control of the error: the updates are more frequent, especially at the beginning of the simulation, and the reduced space is larger at the final time.

We conclude this section with a brief discussion of the computational efficiency of the numerical schemes described above. A plot of the error at the final time vs. the computational time is shown in Figure 15. Several conclusions can be drawn. First, the hyper-reduced model always outperforms its reduced order counterpart as it yields a comparable error at a smaller algorithm runtime. This computational gain is less substantial in the rank-adaptive case because the dimension of the EIM space  $m_\tau$  must also be increased together with the rank of the reduced solution. As mentioned before, this can be addressed by adaptive techniques to select the update frequency  $\Delta$  and the dimension of the EIM space via the tolerance  $\tau_m$ . Finally, using  $r$  rather than  $\theta$  as an error indicator for rank adaptivity proves to be a better choice as the errors are smaller with a slight increase of the computational time.

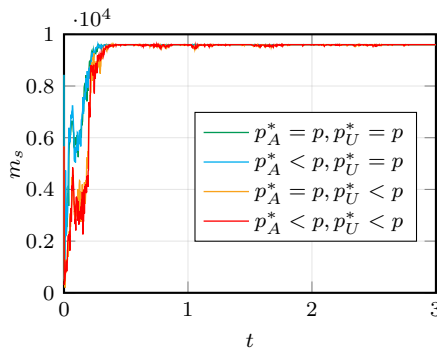


Figure 13: Test 2, non-localized solution. Evolution of the number  $m_s$  of EIM sample indices selected according to Algorithm 1 with  $\tau_{m_s} = 10^{-4}$ .

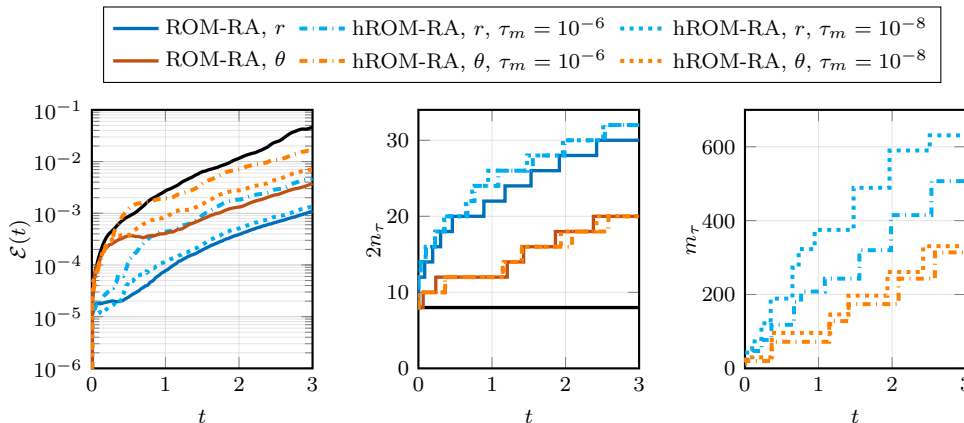


Figure 14: Test 2, non-localized solution. Rank-adaptive case,  $2n_0 = 8$ ,  $\tau_{m_s} = 10^{-4}$ , different error indicators. Left: evolution of the relative errors of the reduced and the hyper-reduced systems. The black solid line refers to the non-rank-adaptive reduced order model (ROM-NRA). Center: evolution of the dimension of the reduced space. Right: evolution of the dimension of the EIM space.

## 9 Concluding remarks

We have developed adaptive hyper-reduced models for Hamiltonian systems that need to be tested for a high number of parameters. The proposed algorithm combines a symplectic dynamical low-rank approximation to approximate the state with an adaptive hyper-reduction strategy to efficiently deal with nonlinear Hamiltonian vector fields. The resulting hyper-reduced models preserve the geometric structure of the Hamiltonian flow and can be solved at a cost that is linear in the dimension  $N$  of the full order model, linear in the number  $p$  of test parameters and that does not depend on the product  $Np$ . Moreover, the adaptivity of the approximate models allows to deal with transport-dominated problems and conservative dynamical systems characterized by slowly decaying Kolmogorov  $n$ -widths. The further adaptivity of both the dimension of the reduced basis space and of the EIM hyper-reduction space allows to achieve the desired accuracy in situations when the (numerical) rank of the solution has high variations over time. The adaptivity is driven by a novel error indicator which, to the best of our knowledge, outperforms the error indicators currently available in the literature, in terms of numerical errors and computational complexity. Finally, we have proposed a strategy to select parameter subsamples for the adaptive components of the algorithm to improve computational efficiency while ensuring favorable approximability properties.

The performances of the proposed rank-adaptive hyper-reduction could be further improved by developing adaptive strategies to select the tolerance  $\tau_m$ , which determines how the dimension of the EIM space changes in time, and the frequency  $\Delta$  at which the EIM space is updated.

## References

- [1] B. M. Afkham and J. S. Hesthaven. “Structure preserving model reduction of parametric Hamiltonian systems”. *SIAM J. Sci. Comput.* 39.6 (2017), A2616–A2644.
- [2] M. Barrault, Y. Maday, N. C. Nguyen, and A. T. Patera. “An ‘empirical interpolation’ method: application to efficient reduced-basis discretization of partial differential equations”. *C. R. Math. Acad. Sci. Paris* 339.9 (2004), pp. 667–672.

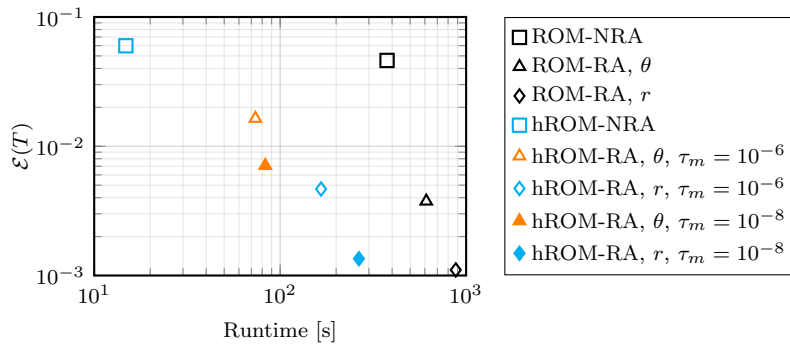


Figure 15: Test 2, non-localized solution. Relative errors at the final time vs. computational time.

- [3] P. Benner, S. Gugercin, and K. Willcox. “A Survey of Projection-Based Model Reduction Methods for Parametric Dynamical Systems”. *SIAM Review* 57.4 (2015), pp. 483–531.
- [4] A. Cannas da Silva. *Lectures on symplectic geometry*. Vol. 1764. Lecture Notes in Mathematics. Springer-Verlag, Berlin, 2001.
- [5] G. Ceruti, J. Kusch, and C. Lubich. “A rank-adaptive robust integrator for dynamical low-rank approximation”. *BIT* 62.4 (2022), pp. 1149–1174.
- [6] A. Charous and P. F. J. Lermusiaux. *Stable rank-adaptive Dynamically Orthogonal Runge-Kutta schemes*. 2023. arXiv: [2211.07852](https://arxiv.org/abs/2211.07852).
- [7] S. Chaturantabut and D. C. Sorensen. “Nonlinear model reduction via discrete empirical interpolation”. *SIAM J. Sci. Comput.* 32.5 (2010), pp. 2737–2764.
- [8] S. Chaturantabut and D. C. Sorensen. “A state space error estimate for POD-DEIM nonlinear model reduction”. *SIAM J. Numer. Anal.* 50.1 (2012), pp. 46–63.
- [9] R. A. DeVore. “The theoretical foundation of reduced basis methods”. *Model reduction and approximation: theory and algorithms*. Society for Industrial and Applied Mathematics, 2017. Chap. 3.
- [10] Z. Drmač and S. Gugercin. “A new selection operator for the discrete empirical interpolation method—improved a priori error bound and extensions”. *SIAM J. Sci. Comput.* 38.2 (2016), A631–A648.
- [11] V. Ehrlicher and D. Lombardi. “A dynamical adaptive tensor method for the Vlasov–Poisson system”. *Journal of Computational Physics* 339 (2017), pp. 285–306.
- [12] J. Frenkel. *Wave mechanics, advanced general theory*. Clarendon Press, Oxford, 1934.
- [13] B. Gao and P.-A. Absil. “A Riemannian rank-adaptive method for low-rank matrix completion”. *Comput. Optim. Appl.* 81.1 (2022), pp. 67–90.
- [14] T. H. Gronwall. “Note on the derivatives with respect to a parameter of the solutions of a system of differential equations”. *Ann. of Math. (2)* 20.4 (1919), pp. 292–296.
- [15] E. Hairer, C. Lubich, and G. Wanner. *Geometric numerical integration*. Second. Vol. 31. Springer Series in Computational Mathematics. Springer-Verlag, Berlin, 2006.
- [16] J. S. Hesthaven and C. Pagliantini. “Structure-preserving reduced basis methods for Poisson systems”. *Math. Comp.* 90.330 (2021), pp. 1701–1740.
- [17] J. S. Hesthaven, C. Pagliantini, and N. Ripamonti. “Rank-adaptive structure-preserving model order reduction of Hamiltonian systems”. *ESAIM Math. Model. Numer. Anal.* 56.2 (2022), pp. 617–650.
- [18] J. S. Hesthaven, C. Pagliantini, and G. Rozza. “Reduced basis methods for time-dependent problems”. *Acta Numerica* 31 (2022), pp. 265–345.
- [19] M. Hochbruck, M. Neher, and S. Schrammer. “Rank-adaptive dynamical low-rank integrators for first-order and second-order matrix differential equations”. *BIT* 63.1 (2023), Paper No. 9, 24.
- [20] O. Koch and C. Lubich. “Dynamical low-rank approximation”. *SIAM J. Matrix Anal. Appl.* 29.2 (2007), pp. 434–454.
- [21] J. E. Marsden and T. S. Ratiu. *Introduction to mechanics and symmetry*. Second. Vol. 17. Texts in Applied Mathematics. Springer-Verlag, New York, 1999.
- [22] A. D. McLachlan. “A variational solution of the time-dependent Schrödinger equation”. *Molecular Phys.* 8 (1964), pp. 39–44.
- [23] E. Musharbash, F. Nobile, and E. Vidličková. “Symplectic dynamical low rank approximation of wave equations with random parameters”. *BIT* 60.4 (2020), pp. 1153–1201.
- [24] M. H. Naderi and H. Babae. “Adaptive sparse interpolation for accelerating nonlinear stochastic reduced-order modeling with time-dependent bases”. *Computer Methods in Applied Mechanics and Engineering* 405 (2023), p. 115813.
- [25] C. Pagliantini. “Dynamical reduced basis methods for Hamiltonian systems”. *Numer. Math.* 148.2 (2021), pp. 409–448.
- [26] C. Pagliantini and F. Vismara. “Gradient-preserving hyper-reduction of nonlinear dynamical systems via discrete empirical interpolation”. *SIAM J. Sci. Comput.* (2023).
- [27] B. Peherstorfer. “Model reduction for transport-dominated problems via online adaptive bases and adaptive sampling”. *SIAM J. Sci. Comput.* 42.5 (2020), A2803–A2836.



- [28] B. Peherstorfer and K. Willcox. “Online adaptive model reduction for nonlinear systems via low-rank updates”. *SIAM J. Sci. Comput.* 37.4 (2015), A2123–A2150.
- [29] L. Peng and K. Mohseni. “Symplectic model reduction of Hamiltonian systems”. *SIAM J. Sci. Comput.* 38.1 (2016), A1–A27.